© 2018. Published by The Company of Biologists Ltd | Development (2018) 145, dev160747. doi:10.1242/dev.160747

RESEARCH ARTICLE

Evolutionarily conserved anterior expansion of the central nervous system promoted by a common PcG-Hox program

Behzad Yaghmaeian Salmani, Ignacio Monedero Cobeta, Jonathan Rakar, Susanne Bauer, Jesús Rodriguez Curt, Annika Starkenberg and Stefan Thor*

ABSTRACT

A conserved feature of the central nervous system (CNS) is the prominent expansion of anterior regions (brain) compared with posterior (nerve cord). The cellular and regulatory processes driving anterior CNS expansion are not well understood in any bilaterian species. Here, we address this expansion in *Drosophila* and mouse. We find that, compared with the nerve cord, the brain displays extended progenitor proliferation, more elaborate daughter cell proliferation and more rapid cell cycle speed in both *Drosophila* and mouse. These features contribute to anterior CNS expansion in both species. With respect to genetic control, enhanced brain proliferation is severely reduced by ectopic Hox gene expression, by either Hox misexpression or by loss of Polycomb group (PcG) function. Strikingly, in PcG mutants, early CNS proliferation appears to be unaffected, whereas subsequent brain proliferation is severely reduced. Hence, a conserved PcG-Hox program promotes the anterior expansion of the CNS. The profound differences in proliferation and in the underlying genetic mechanisms between brain and nerve cord lend support to the emerging concept of separate evolutionary origins of these two CNS regions.

KEY WORDS: Lineage size, Cell cycle, Asymmetric division, Combinatorial control, Nervous system development, Evolution of the CNS

INTRODUCTION

The central nervous system (CNS) is a defining feature of bilaterally symmetric animals (bilateria), and can be generally subdivided into the brain and the nerve cord. The evolution of the CNS from dispersed nerve nets and ganglia in the bilaterian ancestor is under active investigation and thoughtful debate (Holland, 2003; Nielsen, 2012, 2015; Holland et al., 2013; Tosches and Arendt, 2013; Jákely et al., 2015; Arendt et al., 2016; Martín-Durán et al., 2017). Irrespective of its origin, a striking feature, so common as to have been almost unquestioned, is the significant anterior expansion of the brain relative to the nerve cord. This feature is evolutionarily conserved, being evident in annelids, early arthropods and chordates, and becoming increasingly pronounced in vertebrates to reach its zenith in mammals, with the dramatic expansion of the telencephalon. However, the driving forces underlying this size difference are not well understood.

Department of Clinical and Experimental Medicine, Linkoping University, SE-58185 Linkoping, Sweden.

*Author for correspondence (stefan.thor@liu.se)

S.T., 0000-0001-5095-541X

Received 19 October 2017; Accepted 24 February 2018

A regulatory program well-suited for contributing to the establishment of anterior CNS expansion is the Polycomb group (PcG) complex and the Hox homeotic genes. The PcG complex is a collective name for several subcomplexes; Polycomb repressor complexes 1 and 2 (PRC1 and PRC2) have received most attention (Steffen and Ringrose, 2014; Piunti and Shilatifard, 2016). These complexes act to modify key residues in histone tails, with PRC1 ubiquitylating H2A and PRC2 methylating H3K27, resulting in transcriptional repression of target genes. Among the best-known PcG target genes are the Hox homeotic genes, which encode clustered arrays of related transcription factors that play key roles in anterior-posterior (A-P) patterning of the body plan, including the CNS (Garcia-Fernàndez, 2005; Philippidou and Dasen, 2013; Technau et al., 2014; Jung and Dasen, 2015). Strikingly, a common feature in most, if not all, bilateria is the lack of Hox expression in the anterior-most regions of the embryo, including the CNS (Holland et al., 2013; Philippidou and Dasen, 2013), and the PcG complex plays a key role in restricting Hox gene expression to the posterior CNS (Struhl, 1983; Struhl and Akam, 1985; Suzuki et al., 2002; Wang et al., 2002; Isono et al., 2005; Li et al., 2011). Both PcG and Hox genes have been linked to proliferation control, with PcG genes acting in a pro-proliferative and Hox genes in an anti-proliferative manner (Economides et al., 2003; Isono et al., 2005; Zencak et al., 2005; Fasano et al., 2009; Karlsson et al., 2010; Baumgardt et al., 2014; Zemke et al., 2015; Feng et al., 2016; Monedero Cobeta et al., 2017). Both the PcG and Hox homeotic genes are highly conserved, with PcG genes apparent in budding yeast (Jamieson et al., 2013; Dumesic et al., 2015), and Hox genes likely emerging in the common ancestor of Cnidaria-bilateria (Garcia-Fernàndez, 2005; Holland, 2013). Hence, the appearance of the PcG-Hox regulatory program predates the evolution of a bona fide CNS and subsequent emergence of its anterior expansion. However, the involvement of the PcG-Hox regulatory program in promoting anterior CNS expansion has hitherto not been extensively addressed.

The expansion of the anterior CNS could logically be the result of A-P differences in three basic developmental features: the number of progenitors generated in each region along the A-P axis, the extent of programmed cell death (PCD), and the extent of proliferation. Regarding proliferation, this could involve A-P differences in the proliferation of progenitors and/or daughter cells. With respect to daughter cell proliferation, studies in *Drosophila melanogaster* (hereafter *Drosophila*) have revealed three basic modes of daughter cell proliferation, Type 0, I and II, referring to daughter cells that do not divide (Type 0), that divide once (Type I), or that divide multiple times (Type II) (Karcavich and Doe, 2005; Bello et al., 2008; Boone and Doe, 2008; Bowman et al., 2008; Baumgardt et al., 2014; Bertet et al., 2014; Walsh and Doe, 2017). Intriguingly, similar daughter cell proliferation modes have also been identified in the mammalian CNS and are increasingly

Development (2018) 145, dev160747. doi:10.1242/dev.160747

believed to contribute to brain expansion (Kriegstein et al., 2006; Fish et al., 2008; Lui et al., 2011). However, the contribution of PCD and progenitor/daughter cell proliferation to the anterior expansion of the CNS has not been addressed.

Here, we address these issues in *Drosophila* and mouse embryos. Strikingly, in both species the brain shows elevated and extended progenitor and daughter cell proliferation, as well as more rapid cell cycles, compared with the nerve cord. Intriguingly, ectopic expression of Hox genes in the brain, by misexpression or PRC2 mutation, reduces proliferation and lineage size. In contrast, the nerve cord is not affected in PRC2 mutants. Hence, in both *Drosophila* and mouse, we find profound proliferation differences between the brain and nerve cord, which drives anterior CNS expansion. Our findings further suggest that anterior expansion is promoted by an evolutionarily conserved PcG-Hox program.

RESULTS

Gradient of proliferation, cell numbers and lineage size along A-P axis of the *Drosophila* CNS

The *Drosophila* CNS contains 19 segments (Urbach et al., 2016); here, we focus on the brain (B1-B2), thoracic (T2-T3) and abdominal (A8-A10) segments (Fig. 1A). The CNS is generated by ∼1200 neuroblasts (NBs), formed during early to mid-embryogenesis (Fig. 1A) (Doe, 1992; Urbach et al., 2016). In the nerve cord (T1-A10), most NBs initially undergo Type I mode proliferation, during which daughter cells bud off to then divide once into two neurons/glia (Doe, 2008). Subsequently, many NBs undergo a Type I→Type 0 switch such that daughter cells directly differentiate into a neuron/glia (Baumgardt et al., 2014). After a programmed number of divisions, NBs enter quiescence or undergo PCD. PCD plays a major role in removing NBs or neurons/glia, but plays a minimal role in stopping proliferation. In the embryonic brain, these aspects of lineage progression are not as well understood.

Recent studies revealed an A-P gradient in the nerve cord with respect to the Type I→0 switch and NB exit, resulting in an anterior-to-posterior gradient of cell numbers and average lineage sizes (Monedero Cobeta et al., 2017). To determine whether this gradient extends into the brain, we addressed these issues in the B1-B2 segments (Fig. 1B). Proliferating daughter cells and NBs can be distinguished using Dpn, Pros and phosphorylated Ser-10/28 on Histone 3 (PH3) expression patterns; mitotic daughter cells are Dpn^{-}, $PH3^{+}$ and have cytoplasmic Pros, whereas mitotic NBs are Dpn^{+}, $PH3^{+}$ and have asymmetric cortical Pros (Fig. 1C,D) (Baumgardt et al., 2014). B1-B2 NBs delaminate from the neuroectoderm during stage (St) 9-11, and hence we analyzed proliferation in 100-min intervals from St9 to St16+300 min, i.e. just prior to embryo hatching into larva (Fig. 1E). We find that proliferation in B1-B2 commences at St9-St10, first in NBs and then in daughter cells, with continued divisions of both into St16+300 min (Fig. 1E). Addressing the effects of PCD, we noted a striking increase in NB and daughter cell proliferation in PCD mutants [*Df(3L)ED225*] (Fig. 1E). We did not find a significant difference in the numbers of NBs between control and PCD mutants (Fig. S1I). Comparing the B1-B2 proliferation results with previous data for T2-T3 and A8-A10 (Monedero Cobeta et al., 2017), we find elevated proliferation of both daughter cells and NBs in B1-B2, and a substantially prolonged proliferation phase (Fig. 1F,G).

Next, we quantified the total number of cells generated, by DAPI staining at St16+200 min. We found a graded increase in total cell numbers between A8-A10, T2-T3 and B1-B2, and these differences were enhanced in PCD mutants (Fig. 1H; Table S1). Correlating cell numbers with the previously identified number of early NBs (Urbach et al., 2003) and the recently identified Type II NBs (Walsh and Doe, 2017) revealed strikingly different average lineage sizes in the three regions, with B1-B2 lineages being roughly twice as large as T2-T3, and T2-T3 twice as large as A8-A10. These differences were even more pronounced in PCD mutants (Fig. 1I,J).

In summary, we found extended and enhanced NB and daughter cell proliferation in the brain and an apparent absence of the general Type I→0 switch. In addition, in contrast to the nerve cord many brain NBs and daughter cells stop proliferating by undergoing PCD. These brain-specific features combine to drive the generation of substantially larger average lineages and total cell numbers.

Elevated cell cycle gene expression and faster daughter cell cycles in the *Drosophila* brain

The elevated and extended proliferation in the brain, compared with the nerve cord, prompted us to address the nature of the cell cycle in the brain. Both the Type I→0 switch and precise NB exit depend upon balanced expression levels of four key cell cycle genes: the pro-proliferative genes *Cyclin E* (*CycE*), *E2f1*, *string* (*stg*; *Cdc25* in mammals) and the cell cycle inhibitor *dacapo* (*dap*; *Cdkn1a-c* in mammals) (Baumgardt et al., 2014; Bivik et al., 2015). In line with our previous findings in the nerve cord, we observed reduced proliferation in B1-B2 of NBs and/or daughter cells in *CycE*, *stg* and *E2f1* mutants (Fig. S1A-C,E-H). Conversely, *dap* mutants showed elevated proliferation both in a wild-type and PCD mutant background (*dap;ED225*) (Fig. S1A,D,I-K).

Next, we compared immunostaining intensity of these four cell cycle proteins in mitotic NBs of the B1-B2, T2-T3 and A8-A10 segments, scanned in the same embryo fillets, at St13. We found that CycE, E2f1 and Stg immunostaining intensity were significantly higher in B1-B2 compared with T2-T3 and A8-A10 NBs, whereas Dap protein immunostaining intensity did not differ (Fig. 2A-H).

Previous studies in the nerve cord revealed a cell cycle length of ∼40 min for NBs and ∼100 min for daughter cells (Hartenstein et al., 1987; Baumgardt et al., 2014). To address possible A-P differences, we pulsed St13 embryos with 5-ethynyl-2′-deoxyuridine (EdU) for 40 min, to label cycling cells during S phase (Cappella et al., 2008). By staining for EdU, PH3, Pros and Dpn, we determined S→G2→M cell cycle speed of mitotic NBs and daughter cells (Fig. 2P,Q). For B1-B2, T2-T3 and A8-A10 at St13, 10-12% of EdU-labeled NBs were $PH3^{+}$, indicating similar cell cycle speed in NBs along the A-P axis (Fig. 2R). In contrast, the proportion of double-labeled daughter cells in B1-B2 was significantly higher than that in T2-T3 or A8-A10, with the percentage of double-labeled daughter cells in B1-B2 being almost twice as high as that of A8-A10 daughter cells, whereas T2-T3 daughter cells did not differ from A8-A10 (Fig. 2S).

Ectopic expression of *dap* was previously found to trigger the Type I→0 switch prematurely in the nerve cord (Baumgardt et al., 2014). The elevated immunostaining intensity of CycE, E2f1 and Stg in B1-B2 prompted us to test the effects of *dap* misexpression in the brain. However, using the early pan-neural driver *pros-Gal4*, we did not find any effects on daughter cell proliferation in B1-B2 at St15 (Fig. 2K,L,O). In line with previous results in the nerve cord (Baumgardt et al., 2014), NB mitotic index was also unaffected (Fig. 2K,L,N). Considering the elevated levels of CycE, E2f1 and Stg in B1-B2, we analyzed brain proliferation in a cell-cycle sensitized background: triple trans-heterozygotes for *CycE*, *E2f1* and *stg*. Whereas NB proliferation in B1-B2 was not affected in triple trans-heterozygotes, daughter cell proliferation was

Development (2018) 145, dev160747. doi:10.1242/dev.160747

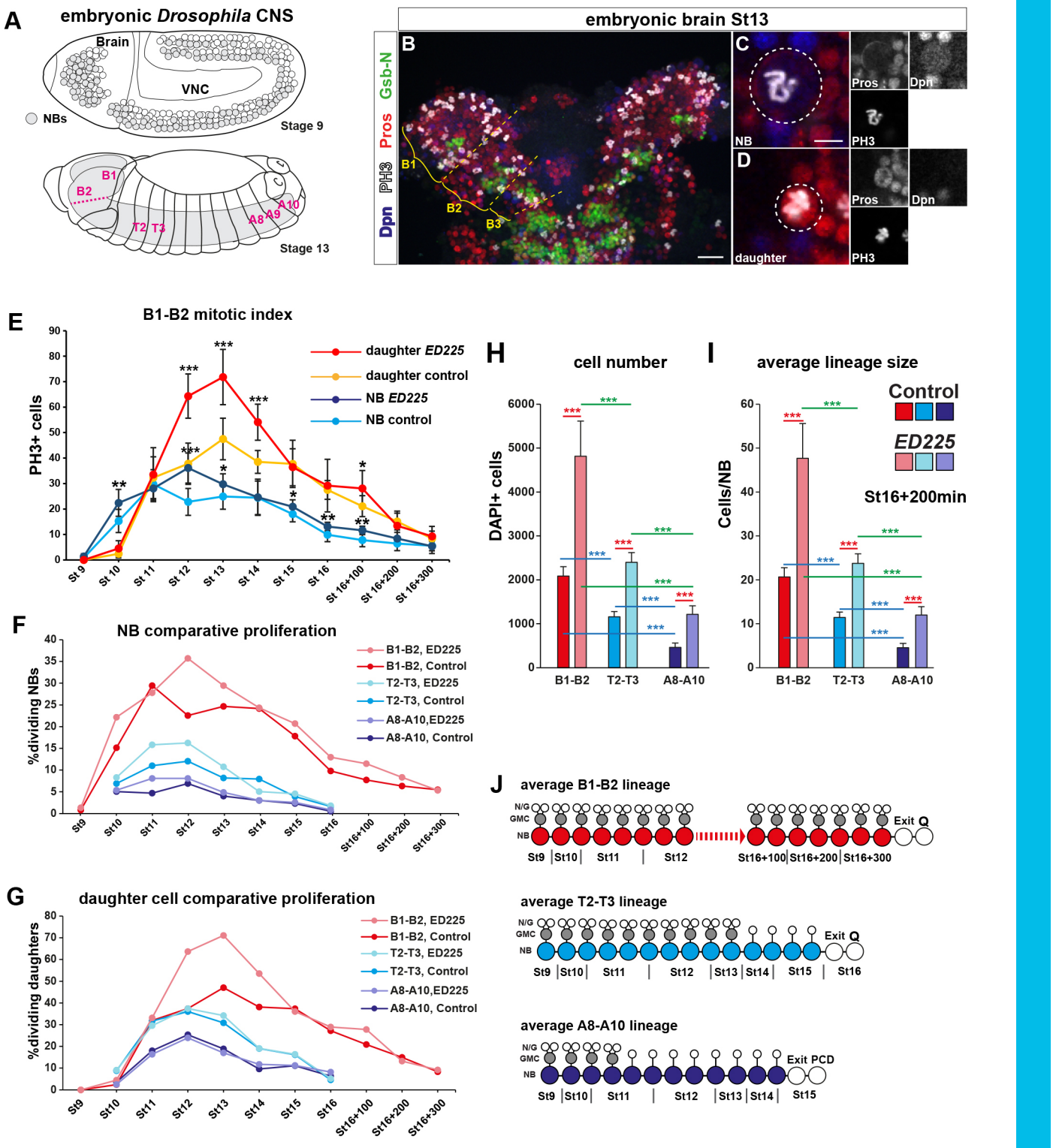

Fig. 1. See next page for legend.

significantly reduced (Fig. 2I,J,N,O). Strikingly, misexpression of *dap* in a triple trans-heterozygote background further reduced daughter cell proliferation (Fig. 2M,O).

We conclude that, similar to the nerve cord, daughter cell and NB proliferation in B1-B2 also depends upon the four key cell cycle genes. However, expression levels of the pro-proliferative cell cycle factors are elevated in the brain, the daughter cell cycles are faster, and there is resistance in daughter cells to cell cycle inhibitor (*dap*) misexpression.

Hox misexpression reduces brain proliferation

Because A-P differences in both proliferation and cell numbers were maintained, even enhanced, in PCD mutants, proliferation control appears to be the crucial mediator of anterior CNS expansion. A

Development (2018) 145, dev160747. doi:10.1242/dev.160747

Fig. 1. The *Drosophila* brain proliferates more than the nerve cord. (A) During *Drosophila* embryonic development ~1200 NBs delaminate from the neuroectoderm during St8-St11, and divide to generate the CNS. The CNS contains 19 segments; herein we focus on B1-B2, T2-T3 and A8-A10. (B) *Drosophila* brain lobes at St13. B1-B3 can be delineated by Gsb-N staining. (C) Mitotic NBs, identified by PH3, Dpn and asymmetric Pros expression. (D) Mitotic daughter cell, identified by PH3, absence of Dpn expression and cytoplasmic localization of Pros. In C and D, dashed lines encircle an NB and a daughter cell in merged panels. (E) Quantification of mitotic NBs and daughter cells in B1-B2 hemi-segments reveals increase in mitotic NBs and daughter cells in PCD mutants compared with control (Student's *t*-test; mean±s.d.; $n \geq 10$ embryos per genotype and stage). (F,G) Percentage of mitotic NBs and daughter cells out of the total number of NBs in each region (B1-B2=101, T2-T3=128 and A8-A10=130) reveals elevated NB and daughter cell proliferation in brain. (H,I) Total cell numbers and average lineage sizes in B1-B2, T2-T3 and A8-A10, in control and PCD mutants, at St16+200 min. Total cell numbers for T2-T3 and A8-A10 segments, adjusted for NB numbers in these segments, compared with B1-B2 hemi-segments (Kruskal–Wallis test; Mann–Whitney *U*-test; mean+s.d.; $n \geq 10$ embryos per genotype and region; red asterisks for control versus *ED225*, blue asterisks for comparison of different segments in control, green asterisks for comparison of different segments in control *ED225* mutants). (J) Model lineage trees based on average lineage size analyses in B1-B2, T2-T3 and A8-A10. GMC, ganglion mother cell; N/G, neuron/glia; Q, quiescence; VNC, ventral nerve cord. *$P \leq 0.05$, **$P \leq 0.01$, ***$P \leq 0.001$. Scale bars: 20 µm (A); 5 µm (C).

likely group of genes underpinning these A-P differences are the Hox homeotic genes, which play key roles during *Drosophila* CNS development (Technau et al., 2014) but are not expressed in the B1-B2 segments (Fig. 3A) (Hirth et al., 1998). Moreover, previous studies demonstrated that the posteriorly expressed Hox gene *Antp*, as well as the three Bithorax complex (BX-C) genes *Ubx*, *abd-A* and *Abd-B*, control the type I→0 switch and NB exit in the nerve cord, creating a gradient of lineage size in the nerve cord (Baumgardt et al., 2014; Monedero Cobeta et al., 2017). We co-misexpressed all three BX-C genes using the *pros-Gal4* driver; a combination that was previously identified as potent in affecting thoracic proliferation (Monedero Cobeta et al., 2017). This resulted in significant reduction of mitotic daughter cells and NBs in B1-B2 (Fig. 3B,C,F,G). To determine whether Hox genes act principally through PCD control, we quantified NB numbers under BX-C misexpression conditions and observed a minor but significant reduction in NB numbers (Fig. S2A). To discriminate between proliferation and PCD, we performed BX-C misexpression in a PCD mutant background. However, we still observed significant reduction of mitotic daughter cells and NBs, even though the effects were weaker (Fig. 3D-G; Fig. S2C). This demonstrates that Hox misexpression affects B1-B2 NB and daughter cell proliferation directly, as well as indirectly by removal of NBs and possibly daughter cells via PCD.

Next, we measured immunostaining intensity of the four key cell cycle proteins in NBs in BX-C-misexpressing embryos, and found that CycE, Stg and Dap intensities were lower, whereas E2f1 intensity did not differ (Fig. 3H-L).

To address the effects of BX-C misexpression upon cell numbers we used DAPI staining to quantify cells in B1-B2 at St16+200 min, using the PCD mutant background to avoid the effect of PCD on cell numbers. As anticipated from the proliferation effects, BX-C misexpression resulted in significantly fewer cells in B1-B2, as well as a smaller average lineage size (Fig. 3M,N; Table S2). The observation of faster daughter cell cycles in the wild-type brain (Fig. 2Q-S) prompted us to investigate whether BX-C misexpression slowed down cell cycles. Although we did not find any effect at St13 (Fig. S2D,E), we observed significant reduction in the percentage of double-labeled daughter cells at St14 (Fig. 3O,P).

To investigate further the effects of BX-C misexpression on the brain, we analyzed expression of two genes selectively expressed in the brain: *Dorsocross2* (*Doc2*; *TBX2/3/6* in human) and *tailless* (*tll*; *Nr2e1* in mammals) (Reim et al., 2003; Kurusu et al., 2009). We quantified Doc2 and Tll protein expression levels in B1-B2 NBs at St13 and observed downregulation of Tll, whereas Doc2 was unaffected (Fig. 3Q; Fig. S2B).

The PcG complex represses Hox expression in the brain and promotes proliferation

Next, we addressed the underlying genetic mechanisms controlling the absence of Hox homeotic genes in the brain. Because the PcG complex is known to restrict Hox homeotic genes to more posterior segments in *Drosophila* (Struhl, 1983; Struhl and Akam, 1985), we analyzed B1-B2 development in maternal-zygotic mutants of *extra sex combs* (*esc*), a core subunit of PRC2, responsible for H3K27 tri-methylation and PcG-mediated repression of target loci (Müller and Verrijzer, 2009). Analyzing H3K27me3 levels in control embryos first, we observed an A-P gradient, with B1-B2 NBs expressing higher levels of H3K27me3 than T2-T3 or A8-A10, and T2-T3 showing higher levels than A8-A10 (Fig. S3A,B). As anticipated, H3K27me3 staining was lost in *esc* maternal-zygotic mutants, and was accompanied by anterior expansion of Antp, Ubx, Abd-A and Abd-B expression into the brain (Fig. 4A-E).

We analyzed proliferation at St11, when there is no detectable Hox expression in NBs (Monedero Cobeta et al., 2017). We found no effect upon the numbers of mitotic NBs or daughter cells in either B1-B2 or A8-A10 in *esc* mutants (Fig. 4F,G). At St13, when Hox expression in NBs is evident (Monedero Cobeta et al., 2017), we observed a reduction in the number of both mitotic NBs and daughter cells in B1-B2 in *esc* mutants, whereas there was no effect in A8-A10 (Fig. 4H,I). To examine the influence of PCD, we quantified proliferation in *esc* mutants in the PCD mutant background. We found a reduction of mitotic NBs and daughter cells in B1-B2 (Fig. S3E,F). In order to exclude the possibility of NB removal by PCD in *esc* mutants, we quantified NB numbers in B1-B2 and A8-A10, in control and *esc* mutant, with or without PCD background, and found no difference between *esc* and control at St13 (Fig. S3C,D).

We quantified immunostaining intensity of the four key cell cycle proteins in B1-B2 NBs in *esc* mutants, and observed reduced intensities of CycE, Stg and E2f1, whereas Dap was increased (Fig. 4J-M,P-S). Transcriptome analysis of control and *esc* mutant whole embryos at St14-15 also revealed significantly reduced expression of these same cell cycle genes (Fig. S3G). We also quantified immunostaining intensity levels of Doc2 and Tll in B1-B2 NBs, and found significant reduction for both proteins in *esc* mutants (Fig. 4N,O,T,U).

Next, we quantified cell numbers, by DAPI staining, and observed a striking reduction of cell numbers in *esc;ED225* mutants compared with *ED225* (control) in B1-B2, whereas no such effects were found in A8-A10 (Fig. 4V; Table S3). Correlating cell numbers to the identified number of NBs revealed strikingly different average lineage sizes between the two genotypes in B1-B2, but not in A8-A10, with *ED225* B1-B2 lineages being twice as large as *esc;ED225* lineages (Fig. 4W). EdU pulsing at St14 revealed a significant reduction in the percentage of EdU-labeled daughter cells that were also $PH3^+$ in B1-B2 of *esc* mutants, whereas no effect was observed in A8-A10 (Fig. 4Y). The proportions of double-labeled NBs were not affected in any region (Fig. 4X).

In summary, the enhanced proliferation observed in the *Drosophila* embryonic brain, compared with the nerve cord, is

Development (2018) 145, dev160747. doi:10.1242/dev.160747

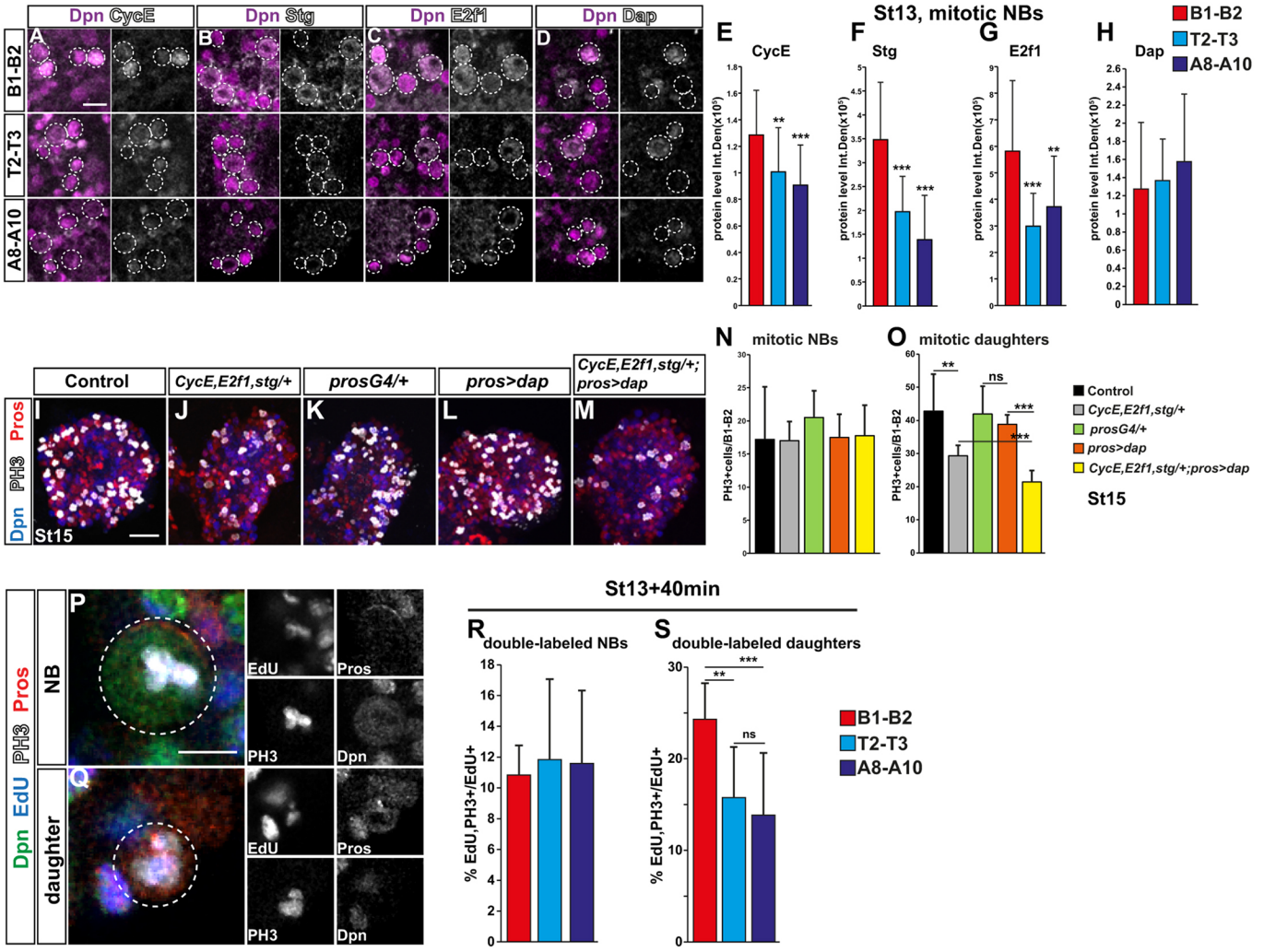

Fig. 2. Expression of cell-cycle genes is elevated in *Drosophila* brain NBs. (A-D) CycE, Stg, E2f1 and Dap expression in NBs (white dashed circles) in B1-B2, T2-T3 and A8-A10 hemi-segments of control embryos at St13. (E-H) Quantification of CycE, Stg and E2f1 levels in mitotic NBs reveals elevated expression in brain, whereas Dap levels were unchanged [integrated density (Int.Den)=area×mean gray value; independent samples Kruskal–Wallis test, Mann–Whitney *U*-test; mean+s.d.; $n \geq 3$ embryos, $n \geq 10$ NBs per region]. (I-M) Mitotic NBs and daughter cells in control, triple trans-heterozygotes, *pros-Gal4/+*, *pros>dap* and *pros>dap* in triple trans-heterozygote background at St15. (N,O) Quantification of mitotic NBs and daughter cells in B1-B2 at St15 (Student's *t*-test; mean+s.d.; $n \geq 10$ embryos per genotype). (P,Q) EdU/PH3 double-labeled NBs and daughter cells (white dashed circles). (R,S) Percentages of EdU/PH3 double-labeled (out of total EdU-labeled) NBs and daughter cells in St13 B1-B2, T2-T3 and A8-A10 hemi-segments. 40 min EdU pulse (one-way ANOVA, Bonferroni post-hoc test; mean+s.d.; $n \geq 10$ embryos per region). $^{**}P \leq 0.01$, $^{***}P \leq 0.001$; ns, not significant. Scale bars: 10 µm (A-D); 20 µm (I-M); 5 µm (P,Q).

sensitive to Hox misexpression and PRC2 mutations, both of which can re-program the brain into a nerve cord-like proliferative profile.

The mouse forebrain has an extended proliferation phase compared with the spinal cord

To study whether our findings from *Drosophila* extend into mammals, we examined neurogenesis and the role of the PcG-Hox program in the developing mouse. We focused on two regions: dorsal telencephalon (Tel) and the spinal cord (SC) at the lumbo-sacral axial level (Fig. 5A). Neurogenesis in the mouse commences around embryonic day (E) 9, and terminates at E14.5 in the SC and E17.5 in the Tel (Caviness et al., 1995; Huang et al., 2013; Kicheva et al., 2014). To analyze proliferation, we used Sox2 as a progenitor/daughter cell marker, PH3 to detect dividing cells, and DAPI to detect all cells, at E11.5, E13.5 and E15.5. Similar to our findings in *Drosophila*, we found that at E11.5 both the Tel and SC had comparable numbers of $PH3^+$ cells/mm^3, as well as a similar percentage of Sox2-expressing cells (Fig. 5B,E,H,I). At E13.5, the SC displayed substantially fewer PH3 cells and a reduction in the percentage of Sox2-expressing cells (Fig. 5F,H,I). This trend continued into E15.5, when the number of PH3 cells was low and only a minor fraction of cells expressed Sox2 (Fig. 5G-I). In contrast, the Tel displayed persistent numbers of PH3 cells from E10.5 to E15.5, and only minor reduction in the number of $PH3^+$ cells and in the percentage of Sox2-expressing cells at E18.5 (Fig. 5C,D,H,I).

In contrast to *Drosophila*, in the mouse there are no identified markers for progenitors and daughter cells common to all axial levels of the CNS. Moreover, there are substantial differences in neurogenesis between the Tel and SC. This relates to the fact that the Tel develops from a neuroepithelial sheet into a multilayered tissue, with a ventricular and subventricular zone, whereas the SC maintains neuroepithelial characteristics during neurogenesis (reviewed by Götz and Huttner, 2005). Moreover, progenitors in the SC only partially develop radial glia cell properties, and retain a broader developmental potential during neurogenesis (Leber and

Development (2018) 145, dev160747. doi:10.1242/dev.160747

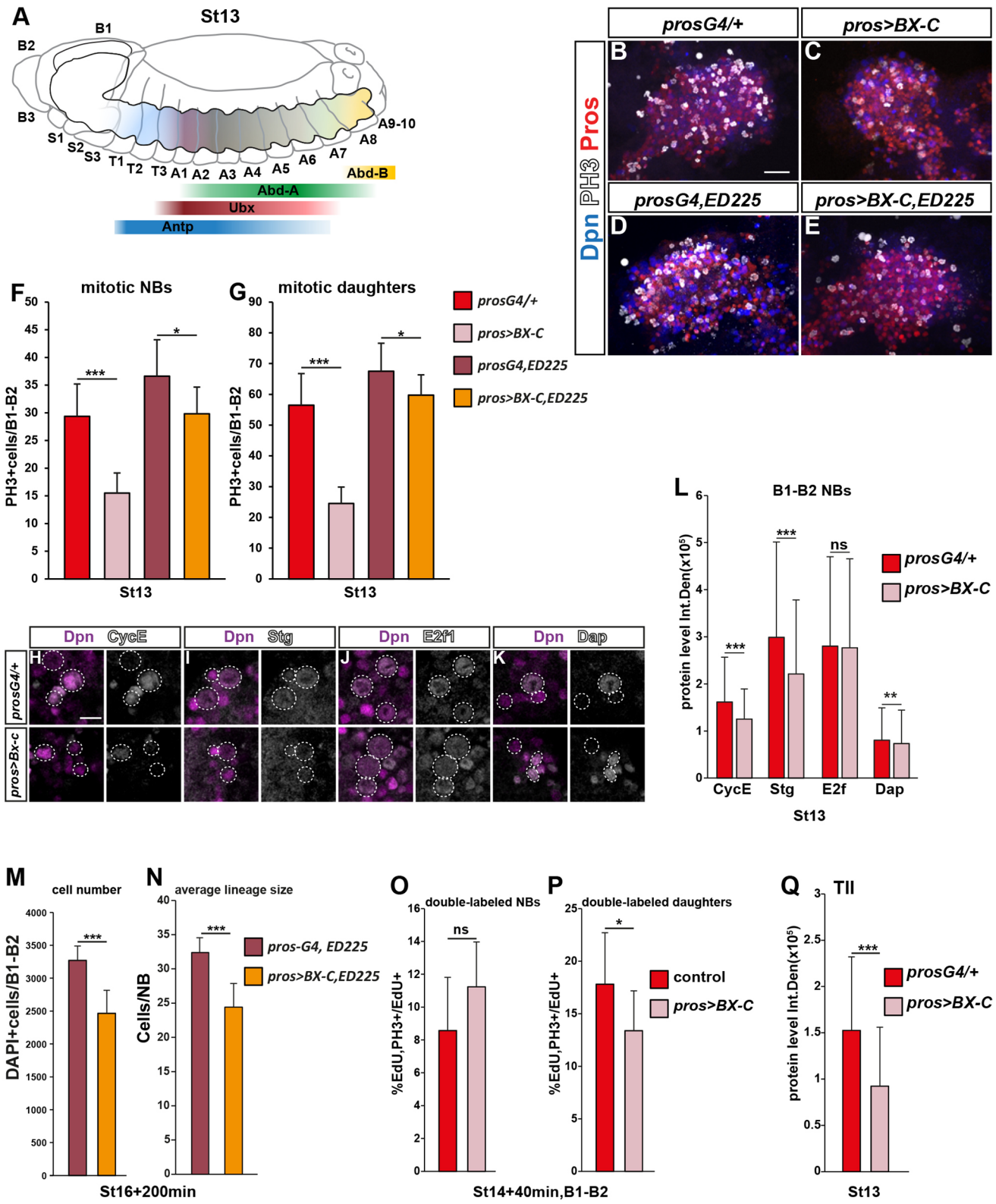

Fig. 3. BX-C Hox misexpression reduces NB and daughter cell proliferation in the *Drosophila* brain. (A) Antp, Ubx, Abd-A and Abd-B expression in embryonic *Drosophila* CNS at St13. (B-E) Mitotic NBs and daughter cells in B1-B2 brain lobes, St13. BX-C misexpression results in reduction of PH3 cells. (F,G) Quantification of mitotic NBs and daughter cells in *prosG4/+*, *pros>BX-C*, *prosG4,ED225* and *pros>BX-C,ED225* St13 B1-B2 (Student's *t*-test; mean+s.d.; $n \geq 10$ embryos per genotype). (H-L) CycE, Stg, E2f1and Dap expression in *prosG4/+* and *pros>BX-C* St13 B1-B2 NBs (white dashed circles) [integrated density (Int.Den)=area×mean gray value; Mann–Whitney *U*-test; mean+s.d.; $n \geq 3$ embryos, $n \geq 225$ NBs per genotype]. (M,N) Quantification of cell numbers and average lineage size in *prosG4,ED225* and *pros>BX-C,ED225* B1-B2, St16+200 min (Student's *t*-test; mean+s.d.; $n \geq 10$ embryos). (O,P) Percentages of EdU/PH3 double-labeled (out of total EdU-labeled) NBs and daughter cells in B1-B2 of St14 control and *pros>BX-C* embryos; 40-min EdU pulse (Student's *t*-test; mean+s.d.; $n \geq 10$ embryos per genotype). (Q) Quantification of TII expression in St13 B1-B2 NBs of *prosG4/+* and *pros>BX-C* embryos (Mann–Whitney *U*-test; mean+s.d.; $n \geq 3$ embryos, $n \geq 271$ NBs). $^{*}P \leq 0.05$, $^{**}P \leq 0.01$, $^{***}P \leq 0.001$; ns, not significant. Scale bars: 20 µm (B-E); 10 µm (H-K).

Development (2018) 145, dev160747. doi:10.1242/dev.160747

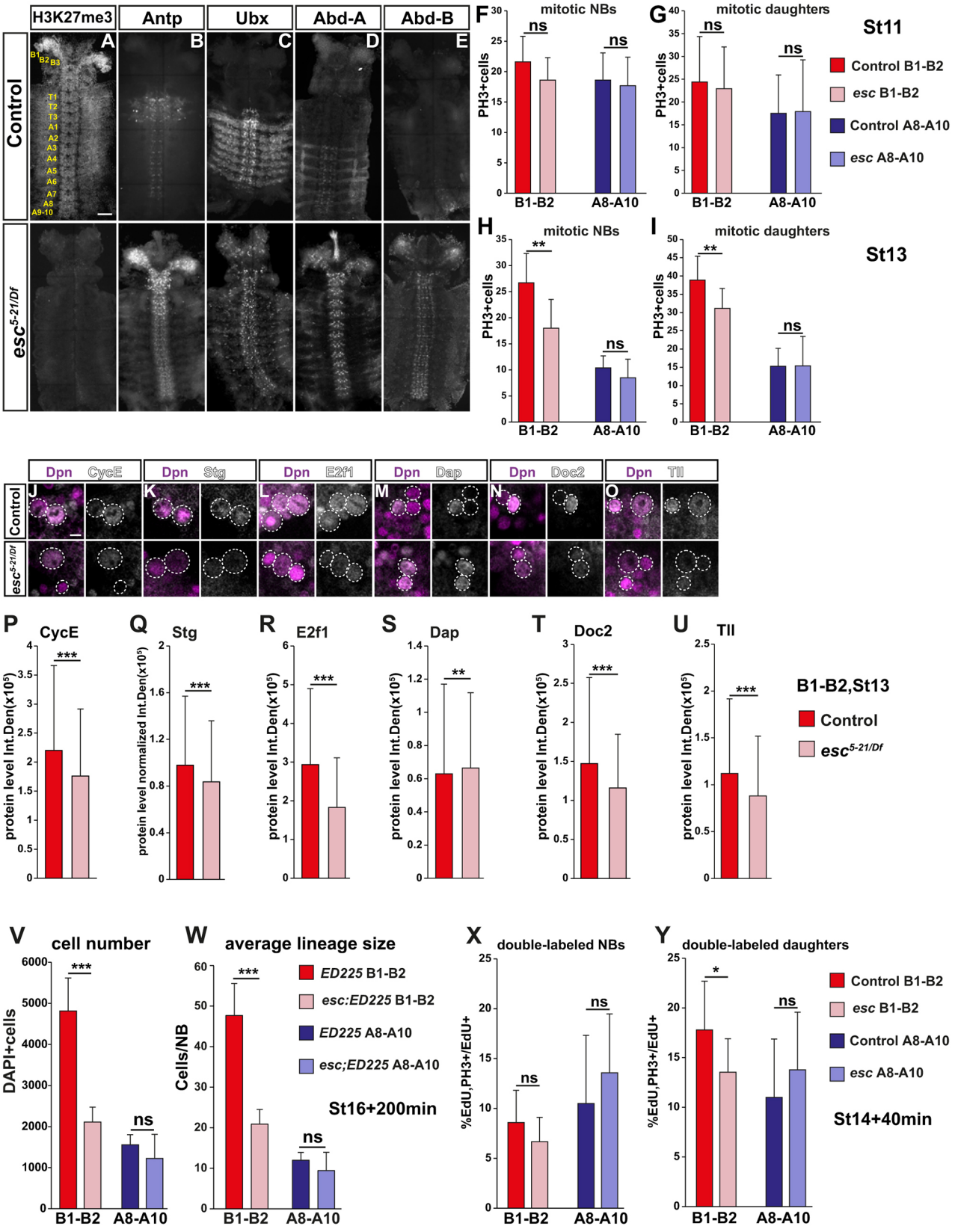

Fig. 4. See next page for legend.

Sanes, 1995). Despite these differences, it is well established that progenitors (radial glia cells and neuroepithelial cells) in both the Tel and SC divide close to the lumen, whereas different types of daughter cells divide further away (Caviness et al., 1995; Kriegstein et al., 2006; Fish et al., 2008; Lui et al., 2011; Kicheva et al., 2014). We therefore analyzed the position of dividing cells in relation to the

Development (2018) 145, dev160747. doi:10.1242/dev.160747

Fig. 4. The PcG complex represses Hox genes in *Drosophila* embryonic brain. (A-E) H3K27me3, Antp, Ubx, Abd-A and Abd-B expression in control and *esc* mutants. (F-I) Quantification of mitotic NBs and daughter cells in St11 and St13 B1-B2 and A8-A10 of control and *esc* embryos (Student's *t*-test; mean+s.d.; $n \geq 10$ embryos). (J-U) CycE, Stg, E2f1, Dap, Doc2 and Tll expression in NBs (white circles) of St13 control and *esc* embryos (Mann–Whitney *U*-test; mean+s.d.; $n \geq 3$ embryos; $n \geq 310$ NBs). (V,W) Cell numbers and average lineage sizes in *ED225* compared with *esc;ED225*, St16+ 200 min, B1-B2 and A8-A10 (Student's *t*-test; mean+s.d.; $n \geq 7$ embryos). (X,Y) Percentages of EdU/PH3 double-labeled (out of total EdU-labeled) NBs and daughter cells in St14 B1-B2 and A8-A10 of control and *esc* embryos (40-min EdU pulse; Student's *t*-test; mean+s.d.; $n \geq 10$ embryos per genotype and region). $^{*}P \leq 0.05$, $^{**}P \leq 0.01$, $^{***}P \leq 0.001$; n.s, not significant. Scale bars: 50 µm (A-E); 5 µm (J-O).

lumen (Fig. S4A). Quantification of the number of cells located further than 20 µm from the lumen revealed that whereas the Tel and SC did not differ at E11.5, at E13.5 and E15.5 the Tel displayed a higher number (Fig. S4B). Defining daughter cells as those dividing outside the 20 µm lumen region, these results suggest elevated daughter cell proliferation in the Tel.

Next, we addressed cell cycle speed in Tel and SC. Twelve-hour EdU pulses at E11 resulted in ratios at E11.5 of ∼0.9 EdU/PH3 double-labeled cells to total $PH3^{+}$ cells in Tel, but only ∼0.5 in SC (Fig. 5K,L). In line with the known reduction in cell cycle speed during neurogenesis, 18-h EdU pulses at late E12 resulted in approximately 50% double-labeled cells in Tel at E13.5, whereas the SC showed only around 10% (Fig. 5L). Hence, for two different EdU pulse lengths, and two different stages, proliferating Tel cells show significantly faster cell cycles that SC.

In *Drosophila*, we noted that the brain expressed more of the four key cell cycle regulators CycE, Stg, Dap and E2f1 than the nerve cord. To determine whether a similar elevation in expression applies to the mouse, we conducted transcriptome analysis of the forebrain and entire SC at E13.5 (Fig. 5A). Intriguingly, we observed elevated expression in the Tel compared with the SC for the orthologous mouse genes: *Ccne1/2* (*CycE*), *Cdc25a/b/c* (*stg*), *Cdkn1a/b* (*dap*) and *E2f1/2/3* (*Ef21*; Fig. 5J), whereas *Cdkn1c* was somewhat reduced. We also noted elevated expression of *Ccna2* (*CycA*) and *Ccnd2* (*CycD*).

In line with previous studies, we find that the Tel has a longer proliferation phase, a greater number of dividing daughter cells, and faster cell cycles than the SC. This is also reflected by elevated cell cycle gene expression in the Tel compared with the SC.

PRC2 mutant mice are microcephalic

Similar to our findings in *Drosophila*, there are several reasons why the Hox homeotic genes are likely candidates for controlling A-P proliferation also in the mouse CNS, for example the fact that the telencephalon does not express any Hox homeotic genes (Philippidou and Dasen, 2013). Moreover, mutation in the *Hoxb13* gene has been shown to trigger excessive proliferation in the SC (Economides et al., 2003). In line with our *Drosophila* studies, we misexpressed *Hoxb9* or *Hoxb13* in the developing chicken telencephalon, by *in ovo* electroporation (Fig. S4C). This resulted in a significant reduction of proliferation in both cases (Fig. 5M,N).

To investigate Hox gene function in vertebrates further, we knocked out PRC2 activity in the mouse as a means of altering Hox expression. Zygotic mutants in *Eed* (the mouse ortholog of *Drosophila esc*) die at E8.5 (Schumacher et al., 1996). Hence, we produced a CNS-specific knockout, by crossing a floxed allele of *Eed* to *Sox1-Cre* (Takashima et al., 2007; Xie et al., 2014) (denoted *Eed-cKO* herein). *Sox1-Cre* crossed to *ROSA26R-EYFP* demonstrated that this Cre strain expresses in the entire CNS, from the E8.5 neuroepithelium and onward to adult (Takashima et al., 2007). Using *Sox1-Cre*, we aimed to achieve early knockout of *Eed* while still allowing embryos to develop until late embryogenesis. Indeed, *Eed-cKO* embryos developed until E18.5 (we did not allow for development until term, and hence cannot judge the survival to term). Moreover, we noted abrogation of PRC2 function from early stages, evident by the selective loss of H3K27me3 in the CNS at E11.5 (Fig. 6C,D, Fig. S5I,J). This was true both for Sox2-positive progenitors and NeuN (Rbfox3)-positive postmitotic cells (Fig. S5K,L). A minor subset of cells in the CNS remained H3K27me3 positive in the knockout, but IB4 staining identified them as vascular cells (Stubbs et al., 2009) (Fig. S5A-D). One day earlier, at E10.5, we noted positive staining for H3K27me3 in both SC and Tel (Fig. S5E-H). Thus, despite *Sox1-Cre* being active already at E8.5, loss of the H3K27me3 mark occurs between E10.5 and E11.5.

At E15.5, we noted reduction in size of the Tel in *Eed-cKO*, whereas the SC appeared morphologically unaffected (Fig. 6A). The reduced size of the Tel became even more apparent at E18.5 (Fig. 6B). We analyzed proliferation by Sox2, PH3 and DAPI staining. Focusing on the Tel first, we noted that initial stages of neurogenesis (E11.5) were apparently unaffected in *Eed-cKO*, evident by the number of $PH3^{+}$ cells/mm^3, the percentage of Sox2-expressing cells, and the number of dividing daughter cells/mm^2 of lumen area (Fig. 6G,H; Fig. S6A-D). However, at E13.5, E15.5 and E18.5 in *Eed-cKO* we observed fewer $PH3^{+}$ cells/mm^3, a reduction of the percentage of Sox2-expressing cells, and a reduction of the number of dividing daughter cells/mm^2 of lumen area (Fig. 6E-H; Fig. S6A-D). None of these proliferation parameters was affected in the SC in *Eed-cKO* at E10.5, E11.5, E13.5 or E15.5 (Fig. 6G,H; Fig. S6E-H).

Next, we analyzed the expression of $p27^{KIP1}$ (p27, also known as Cdkn1b; *Drosophila* Dap), E2F3 (*Drosophila* E2f1) and Cdc25C (*Drosophila* Stg). In control Tel at E11.5, p27 expression was mostly observed in cells located at the outer layer of Sox2 cells, with most p27 cells being Sox2 negative (Fig. S7A,B). In *Eed-cKO*, we found that although p27 expression was not obviously upregulated, we noted more p27-expressing cells within the Sox2 layer (Fig. S7C,D). At E13.5, this effect was more pronounced, and additionally the outer layer of $p27^{+}$ $Sox2^{-}$ cells was greatly expanded (Fig. S7E-H). At E15.5, p27 was restricted to the outer layer in control Tel, whereas in *Eed-cKO* the outer $p27^{+}$ $Sox2^{-}$ layer spanned most of the developing Tel (Fig. S7I-L). E2F3 and Cdc25C expression in Sox2 cells in Tel showed a tendency for reduced expression, but this was not significant (Fig. S8A-F). However, analysis of Sox2/PH3 cells and Sox2 cells within 20 µm from the lumen showed a significant reduction for E2F3, whereas Cdc25C was still not affected (Fig. S8G-N).

Next, we performed 24-h EdU pulses at E14.5 and analyzed at E15.5. This revealed a near-complete loss of EdU incorporation in the *Eed-cKO* Tel compared with control (Fig. S7I-L). To address the possible involvement of PCD in the reduction of Tel size, we stained for cleaved-caspase 3 (CC3). We found that whereas control Tel had very few CC3 cells at E11.5, the *Eed-cKO* Tel displayed a number of CC3-expressing cells (Fig. S7M-P). At E13.5, CC3 expression was robust in both control and *Eed-cKO*. However, in control Tel CC3 cells were mostly confined to the outer (Sox2-negative) layer whereas the *Eed-cKO* displayed CC3-expressing cells throughout the Sox2 layer (Fig. S7Q-T). At E15.5, strikingly, whereas control expressed CC3 in a similar profile as observed at E13.5, the *Eed-cKO* showed an almost complete absence of CC3 cells (Fig. S7U-X).

Development (2018) 145, dev160747. doi:10.1242/dev.160747

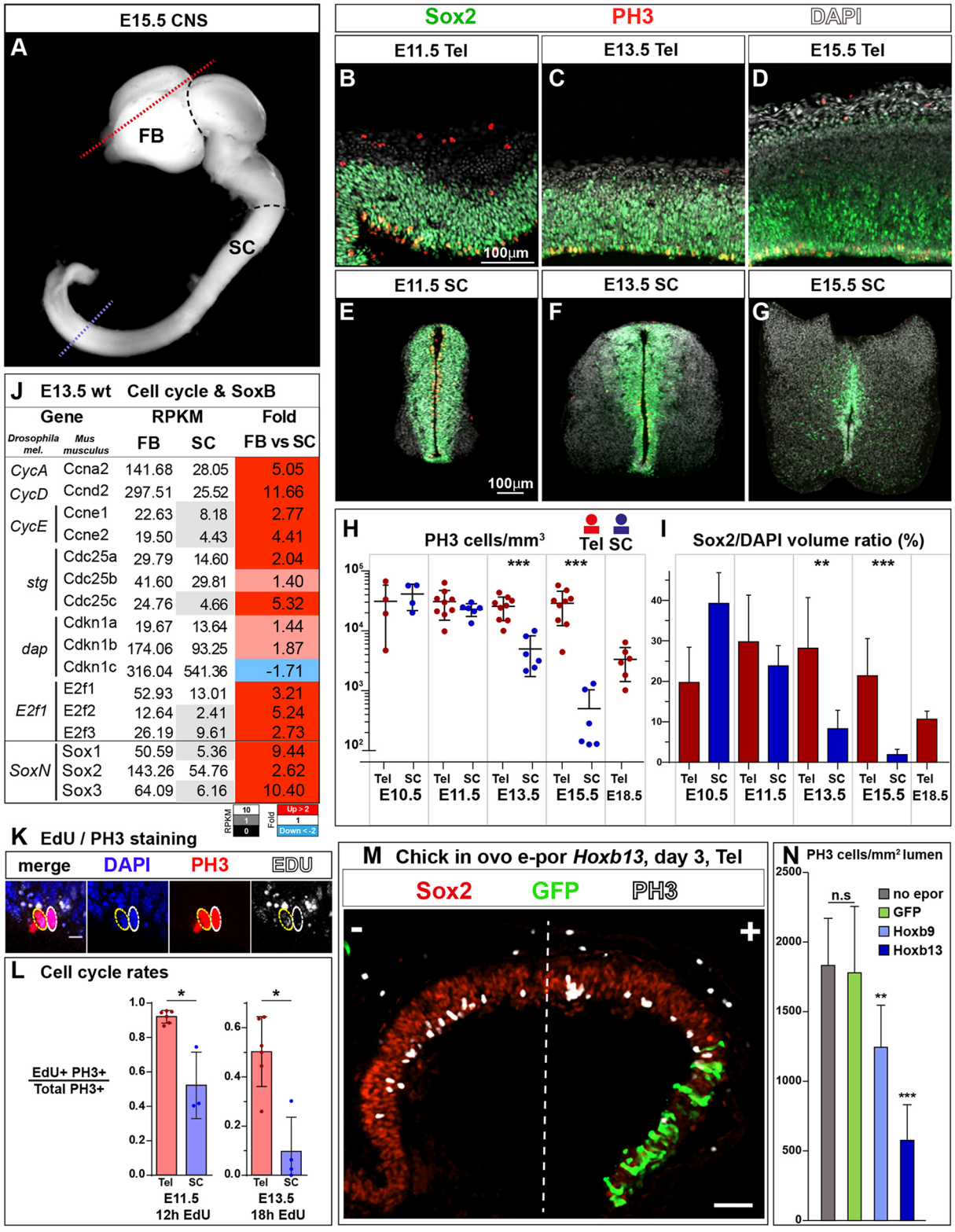

Fig. 5. Extended proliferation in mouse telencephalon compared with spinal cord. (A) E15.5 mouse CNS subdivided into forebrain (FB) and spinal cord (SC). (B-G) Sox2, PH3 and DAPI staining of telencephalon sections (Tel; upper panels) and spinal cord (SC; lower panels) of E11.5, E13.5 and E15.5 control mouse embryos. (H,I) Quantification of mitotic cells per mm^3, and Sox2/DAPI volume ratios, in Tel and SC (Mann–Whitney; mean±s.d.; $n \geq 3$ embryos; *y*-axis scale in H is log10). Proliferation (PH3) and the number of progenitors (Sox2) are both significantly reduced in the SC at E13.5 and E15.5, compared with Tel. (J) RNA-seq analysis of cell-cycle genes in the FB and SC of E13.5 control embryos. (K) Representative image of single- (white circle) and double-stained (yellow circle) PH3/EdU cells. (L) Cell cycle rates in Tel and SC, at E11.5 and E13.5 (ratio of double-labeled EdU/PH3 cells to total PH3-labeled cells). (M) Day 3 chick Tel electroporated with *Hoxb13* and *GFP* plasmids, stained for Sox2, GFP and PH3 on horizontal sections. (N) Quantification of mitotic cells/mm^2 of Tel lumen area in the non-electroporated (no epor) control side, *GFP*-electroporated control, *Hoxb9+GFP* and *Hoxb13+GFP*, in day 3 embryos (Student's *t*-test; mean+s.d.; $n \geq 3$ embryos). Scale bars: 100 µm (B-G); 10 µm (K); 50 µm (M).

Development (2018) 145, dev160747. doi:10.1242/dev.160747

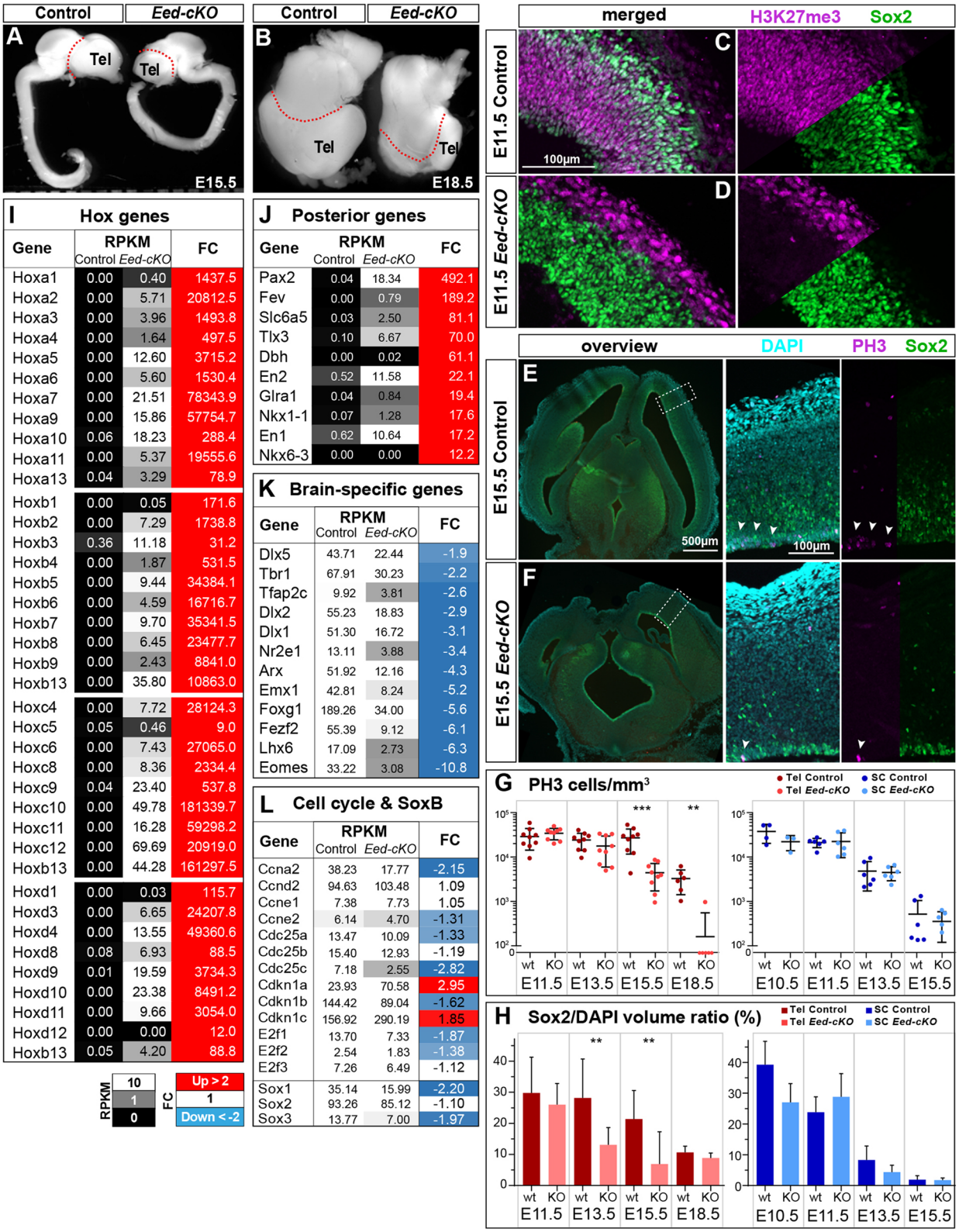

I Hox genes

Gene	RPKM Control	RPKM *Eed-cKO*	FC
Hoxa1	0.00	0.40	1437.5
Hoxa2	0.00	5.71	20812.5
Hoxa3	0.00	3.96	1493.8
Hoxa4	0.00	1.64	497.5
Hoxa5	0.00	12.60	3715.2
Hoxa6	0.00	5.60	1530.4
Hoxa7	0.00	21.51	78343.9
Hoxa9	0.00	15.86	57754.7
Hoxa10	0.06	18.23	288.4
Hoxa11	0.00	5.37	19555.6
Hoxa13	0.04	3.29	78.9
Hoxb1	0.00	0.05	171.6
Hoxb2	0.00	7.29	1738.8
Hoxb3	0.36	11.18	31.2
Hoxb4	0.00	1.87	531.5
Hoxb5	0.00	9.44	34384.1
Hoxb6	0.00	4.59	16716.7
Hoxb7	0.00	9.70	35341.5
Hoxb8	0.00	6.45	23477.7
Hoxb9	0.00	2.43	8841.0
Hoxb13	0.00	35.80	10863.0
Hoxc4	0.00	7.72	28124.3
Hoxc5	0.05	0.46	9.0
Hoxc6	0.00	7.43	27065.0
Hoxc8	0.00	8.36	2334.4
Hoxc9	0.04	23.40	537.8
Hoxc10	0.00	49.78	181339.7
Hoxc11	0.00	16.28	59298.2
Hoxc12	0.00	69.69	20919.0
Hoxb13	0.00	44.28	161297.5
Hoxd1	0.00	0.03	115.7
Hoxd3	0.00	6.65	24207.8
Hoxd4	0.00	13.55	49360.6
Hoxd8	0.08	6.93	88.5
Hoxd9	0.01	19.59	3734.3
Hoxd10	0.00	23.38	8491.2
Hoxd11	0.00	9.66	3054.0
Hoxd12	0.00	0.00	12.0
Hoxb13	0.05	4.20	88.8

J Posterior genes

Gene	RPKM Control	RPKM *Eed-cKO*	FC
Pax2	0.04	18.34	492.1
Fev	0.00	0.79	189.2
Slc6a5	0.03	2.50	81.1
Tlx3	0.10	6.67	70.0
Dbh	0.00	0.02	61.1
En2	0.52	11.58	22.1
Glra1	0.04	0.84	19.4
Nkx1-1	0.07	1.28	17.6
En1	0.62	10.64	17.2
Nkx6-3	0.00	0.00	12.2

K Brain-specific genes

Gene	RPKM Control	RPKM *Eed-cKO*	FC
Dlx5	43.71	22.44	-1.9
Tbr1	67.91	30.23	-2.2
Tfap2c	9.92	3.81	-2.6
Dlx2	55.23	18.83	-2.9
Dlx1	51.30	16.72	-3.1
Nr2e1	13.11	3.88	-3.4
Arx	51.92	12.16	-4.3
Emx1	42.81	8.24	-5.2
Foxg1	189.26	34.00	-5.6
Fezf2	55.39	9.12	-6.1
Lhx6	17.09	2.73	-6.3
Eomes	33.22	3.08	-10.8

L Cell cycle & SoxB

Gene	RPKM Control	RPKM *Eed-cKO*	FC
Ccna2	38.23	17.77	-2.15
Ccnd2	94.63	103.48	1.09
Ccne1	7.38	7.73	1.05
Ccne2	6.14	4.70	-1.31
Cdc25a	13.47	10.09	-1.33
Cdc25b	15.40	12.93	-1.19
Cdc25c	7.18	2.55	-2.82
Cdkn1a	23.93	70.58	2.95
Cdkn1b	144.42	89.04	-1.62
Cdkn1c	156.92	290.19	1.85
E2f1	13.70	7.33	-1.87
E2f2	2.54	1.83	-1.38
E2f3	7.26	6.49	-1.12
Sox1	35.14	15.99	-2.20
Sox2	93.26	85.12	-1.10
Sox3	13.77	7.00	-1.97

Fig. 6. Telencephalon development is perturbed in *Eed-cKO* mouse embryos. (A) CNS of E15.5 control and *Eed-cKO* embryos. Whereas the *Eed-cKO* Tel is severely reduced in size, the SC is not apparently affected. (B) E18.5 control and *Eed-cKO* brains. The difference in Tel size between the KO and control is further pronounced. (C,D) Sox2 and H3K27me3 in horizontal sections of E11.5 control (top, projection=27 µm) and *Eed-cKO* (bottom, projection=33 µm) Tel. Left panels show merge. (E,F) Left: horizontal sections of E15.5 control (top) and *Eed-cKO* (bottom). Middle and right: high magnification images of the area of interest (boxed on the left) PH3, DAPI and Sox2 staining. Arrowheads indicate mitotic cells. (G,H) Quantification of mitotic cells per mm^3 and Sox2/DAPI volume ratios of Tel and SC tissues of control and *Eed-cKO* embryos (Mann–Whitney; mean±s.d.; $n \geq 3$ embryos: *y*-axis scale in G) is log10). (I-L) RNA-seq analysis of Hox, posterior-, brain-specific, cell-cycle and SoxB genes, in the Tel of E15.5 control and *Eed-cKO* embryos (n=2 embryos). FC, fold change. Red indicates FC>2, white FC=1, blue FC<2.

Development (2018) 145, dev160747. doi:10.1242/dev.160747

In contrast to the effects in Tel, SC showed no apparent effects in immunostaining intensity for p27 or CC3 (Fig. S9A-L).

To investigate development of the Tel further, we stained for Tbr2 (Eomes) and Tbr1, which mark daughter cells and neurons, respectively (Englund et al., 2005). At E11.5, we observed an apparently normal representation of both markers, whereas at E13.5 and E15.5, there was a gradual reduction in Tbr2 cells and an apparent premature increase in Tbr1 cells (Fig. S10A-L, Fig. S11).

In summary, *Eed-cKO* embryos display a truncated developmental program in the Tel, with premature reduction of the Sox2 proliferative zone, fewer PH3 cells, reduction of EdU incorporation, elevated p27 expression and premature onset of PCD (Fig. S11). These events likely underlie the markedly reduced size of the Tel. In contrast, none of these markers is affected in the SC in *Eed-cKO*.

Transcriptome analysis shows that the forebrain is posteriorized in PRC2 mutants

To investigate the mechanistic basis for the microcephalic phenotype, we analyzed the transcriptome in the E15.5 forebrain (FB), in control and *Eed-cKO* embryos. As anticipated, in control FB we did not observe expression of any of the Hox homeotic genes, supporting the notion of the wild-type FB as a Hox-free region [reads per kilobase of transcript per million mapped reads (RPKMs) near, or below, detection level] (Fig. 6I). In contrast, *Eed-cKO* FB showed ectopic expression of all 39 Hox-genes (Fig. 6I). A number of other genes with more posterior CNS expression (SC, hindbrain) were also upregulated in *Eed-cKO* (*Pax2*, *Fev*, *En1/2*) (Fig. 6J). In contrast to the upregulation of Hox and other posterior genes, a number of well-studied brain-specific developmental control genes were downregulated in *Eed-cKO* (*Dlx1/2/5*, *Tbr1*, *Nr2e1*, *Arx*, *Emx1*, *Foxg1*, *Fezf2*, *Tbr2*) (Fig. 6K). Finally, analysis of core cell cycle genes also revealed downregulation in *Eed-cKO* FB of several pro-proliferative genes and, conversely, upregulation of the cell cycle inhibitor genes *Cdkn1a* and *Cdkn1c* (Fig. 6L).

These transcriptome results revealed a comprehensive re-programming of the FB into a more posterior CNS identity in *Eed-cKO*, evident by ectopic expression of Hox and posterior genes, downregulation of brain-specific genes, and an accompanying re-programming of cell cycle gene expression.

DISCUSSION

Conserved A-P differences in progenitor and daughter cell proliferation contributes to anterior CNS expansion

Previous studies identified a gradient of NB exits and Type I→0 daughter cell proliferation switches in the *Drosophila* nerve cord (Monedero Cobeta et al., 2017). Here, we find that this gradient extends into the brain, where it is accentuated, and we find no evidence for a general Type I→0 switch in the brain. In line with the enhanced brain proliferation, the even more proliferative Type II daughter mode has only been described in a subset of NBs in the B1 part of the brain (Bello et al., 2008; Boone and Doe, 2008; Bowman et al., 2008; Walsh and Doe, 2017). In the nerve cord, PCD plays a minor role in stopping NB and daughter cell proliferation (Monedero Cobeta et al., 2017). In contrast, we find that it is a prevalent stopping mechanism in the brain. Hence, surprisingly, PCD does not contribute to the anterior expansion of the CNS, but rather counteracts it. We find elevated levels of CycE, Stg and E2f1 in the brain, as well as faster daughter cell cycles, compared with thorax and abdomen. This 'super-charging' of the cell cycle also manifests itself in resistance to *dap*-mediated Type I→0 switch, evident from a lack of *dap* misexpression effects in control, whereas the *CycE*, *stg*, *E2f1* triple heterozygotes sensitized background was affected. These features combine to generate radically different lineage sizes along the A-P axis.

In the mouse, proliferation continues for a longer time in the brain than the SC (Caviness et al., 1995; Huang et al., 2013; Kicheva et al., 2014). In fact, there is continuing adult proliferation in some regions of the brain (Gage and Temple, 2013; Bergmann et al., 2015), something that has not been described for the SC. During mammalian neurogenesis, progenitors (radial glia cells) generate daughter cells that can directly differentiate, divide once, or divide multiple times (Franco and Müller, 2013). Hence, in spite of substantial evolutionary distance, alternate daughter cell proliferation, reminiscent of the *Drosophila* Type 0, I and II modes, is evident also in mammals. Intriguingly, the repertoire of dividing daughter cells appears to have expanded from the three basic modes observed in *Drosophila*, and a number of different types have been identified (Lui et al., 2011; Betizeau et al., 2013). The identity of different types of proliferating daughter cells, identified in different mammalian species, is still debated (Martínez-Cerdeño and Noctor, 2016). However, there is little, if any, evidence for more proliferative daughter cells, akin to *Drosophila* Type II NBs and mammalian basal progenitors, in the mouse SC. The lack of specific progenitor and daughter cell markers along the entire A-P axis precluded us from conducting a systematic mitotic index analysis in the mouse, such as we conducted in *Drosophila*. However, based upon the distance to the lumen, we found that dividing daughter cells were more prevalent in the Tel compared with the SC, at E13.5 and E15.5. In addition, EdU/PH3 double-labeling revealed faster cell cycles in the Tel compared with the SC. The enhanced proliferation in the brain, compared with the SC, was further mirrored by our finding of elevated levels of cyclin D2, cyclin E1/2, Cdc25a/b/c (*Drosophila* Stg) and E2F1/2/3 in the brain.

To summarize, in both *Drosophila* and mouse, the brain displays an extended proliferation period, elevated cell cycle gene expression, more rapid cell cycles, and more elaborate daughter cell proliferation modes. These features act in concert to promote the anterior expansion of the CNS (Fig. 7A-D).

The PcG complex excludes Hox expression from the brain and promotes proliferation

In *Drosophila*, previous studies demonstrated that Hox genes are key players in controlling lineage size along the nerve cord A-P axis, by triggering both the Type I→0 switch and NB exit (Karlsson et al., 2010; Baumgardt et al., 2014; Monedero Cobeta et al., 2017). The brain is notable for its lack of Hox homeotic gene expression, an evolutionarily conserved feature (Holland et al., 2013; Philippidou and Dasen, 2013). In line with these findings, we find that misexpression of Hox genes in the *Drosophila* brain changes cell cycle gene expression, and triggers premature Type I→0 switches and NB exit. This is logically accompanied by reductions in total cell number and average lineage size.

In *esc* maternal/zygotic mutants, we find that H3K27me3 is lost, Hox gene expression expands anteriorly into the brain, and there is downregulation of brain-specific regulators, e.g. Doc1 and Tll. This is accompanied by cell cycle gene expression changes, aberrant Type I→0 switches and premature NB exit, resulting in dramatic reductions in total cell number and average lineage size; strikingly, B1-B2 average lineage size in *esc* mutants is equivalent to that of wild-type abdominal segments.

In the mouse CNS, the involvement of Hox homeotic gene regulation in proliferation control is not as well established as in

Development (2018) 145, dev160747. doi:10.1242/dev.160747

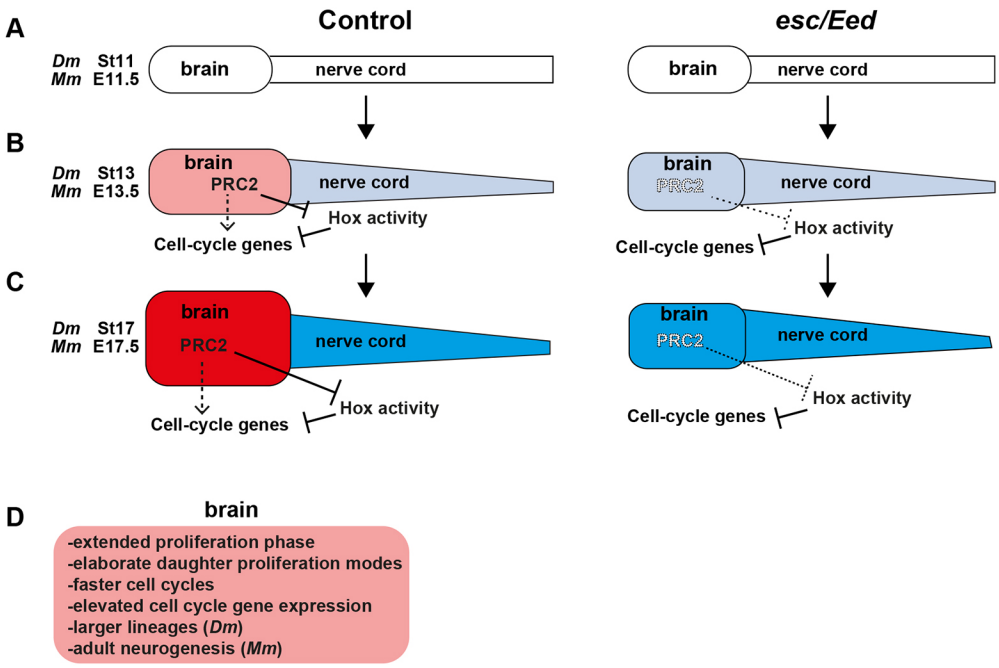

Fig. 7. Evolutionarily conserved PcG-Hox program promotes anterior CNS expansion. (A) Early stages of CNS development in control and PRC2 mutant *Drosophila* (*Dm*) and mouse (*Mm*) embryos. PRC2 mutants display only minor effects upon early CNS development. (B) With increasingly robust Hox activity, PRC2 activity becomes crucial for repressing Hox gene expression in the brain, thereby ensuring expansion of the anterior CNS. PRC2 also directly, or indirectly, ensures high cell-cycle gene expression. In the nerve cord, Hox-mediated suppression of cell-cycle genes contributes to lower proliferation. (C) The effects of PRC2 mutation becomes more pronounced towards the end of CNS development, when brain size expansion peaks and depends even more upon Hox repression. (D) The brain in *Drosophila* and mouse displays a number of unique features compared with the nerve cord.

Drosophila. However, one striking example stems from studies of *Hoxb13* mutants, which displayed a marked increase in proliferation in the posterior spinal cord (Economides et al., 2003). Similarly, we find that misexpression of *Hoxb9* and *Hoxb13* in the chick telencephalon results in reduced proliferation, lending further support for a close connection between Hox genes and proliferation. Similar to *Drosophila*, mutating PcG components in the mouse results in anterior expansion of Hox gene expression (Suzuki et al., 2002; Wang et al., 2002; Isono et al., 2005; Li et al., 2011). Reduced proliferation has also been demonstrated in different PcG mouse mutants (Isono et al., 2005; Zencak et al., 2005; Fasano et al., 2009; Zemke et al., 2015; Feng et al., 2016). However, probably owing to the use of hypomorphic alleles, genetic redundancy, and late or restricted *Cre*-deleter strains, the described effects upon brain development did not appear to be as profound as those observed herein. Targeting the PRC2 component *Eed* (*Drosophila esc*) and deleting it using the early and pan-neuroectodermal *Sox1-Cre* line, we find that H3K27me3 is lost from the entire developing CNS from early stages onwards. This results in striking upregulation of Hox genes and posterior patterning genes in the brain, as well as downregulation of brain-specific genes. We also noted downregulation of pro-proliferative and upregulation of anti-proliferative cell cycle genes. This is accompanied by dramatic reduction of the proliferative zone, evident by fewer Sox2 cells, reduced progenitor and daughter cell proliferation, and reduction in overall Tel size.

The downregulation of brain-specific regulatory genes in *esc*/*Eed* mutants raises the possibility that reduced proliferation may, at least in part, result from the role that these genes play during brain development. However, it should be pointed out that none of these genes is completely downregulated in PcG mutants, in either species. Similarly, it is possible that the reduced proliferation observed in PcG mutants may be, at least in part, caused by increased PCD. In *Drosophila*, we can rule this out by using the PCD mutant *ED225*, which revealed that proliferation was still severely affected in *ED225, esc* double mutants. However, in the mouse, as we are unaware of genetic tools that completely remove PCD in the developing CNS, the contribution of PCD of, for example, progenitors remains a possible contributing factor.

We find no indication that mutation of *esc*/*Eed* affects early aspects of CNS proliferation. This is evident in *Drosophila esc* mutants by normal NB numbers in B1-B2 and apparently normal early brain proliferation (St11). Hence, the higher number of NBs normally generated in brain segments (e.g. 144 for the entire B1 segment versus 64 for most thoracic and abdominal segments) provides part of the driving mechanisms behind the anterior expansion, and this aspect does not appear to be controlled by the PcG-Hox program. Similarly, in mouse *Eed-cKO* embryos we observe apparently normal early Tel development and proliferation (E11.5). This lack of apparent effects on early Tel proliferation in *Eed-cKO* may explain why the Tel still retains some degree of its prominent size at all stages examined (Fig. 6A,B). It is of course also likely that other mechanisms, acting independently of PcG-Hox, play a role herein. In line with studies of other PRC2 components (Zemke et al., 2015; Feng et al., 2016), other brain regions may also be affected in *Eed-cKO*, but this awaits further study. Intriguingly, our results on the SC shows that proliferation is not affected at any stage examined, supporting the notion of brain-specific proliferation effects of the PcG-Hox program.

Brain and nerve cord – separate parts fused together during evolution?

Our study and others outlined herein point to profound differences between brain and nerve cord neurogenesis in both *Drosophila* and mouse that drive the anterior expansion of the CNS. Our results indicate that this is promoted by a conserved PcG-Hox program. These findings raise the question of why two regions of the same tissue develop according to such different principles.

One explanation may be provided by considering the common ancestor of bilateria and their closest relative group, the Cnidaria (e.g. jellyfish). Recent studies of phylogeny and gene expression have led to the proposal that the CNS evolved by the merging of two separate nervous systems present in the common ancestor: the apical and basal nervous systems (ANS and BNS) (Nielsen, 2012, 2015;

Development (2018) 145, dev160747. doi:10.1242/dev.160747

Tosches and Arendt, 2013; Arendt et al., 2016). Intriguingly, even in arthropods, e.g. *Drosophila*, the brain and nerve cord initially develop separately, and merge during subsequent embryogenesis (Fig. 1A). The PcG complex appeared early in evolution, and is present in fungi, whereas the Hox homeotic genes appeared later, but are apparent both in Cnidaria and early bilateria (Garcia-Fernàndez, 2005; Holland, 2013; Jamieson et al., 2013; Dumesic et al., 2015). The complexity of both the PcG and Hox systems dramatically increased (Garcia-Fernàndez, 2005; Müller and Verrijzer, 2009; Holland, 2013; Piunti and Shilatifard, 2016), and this increased complexity mirrors the formation and evolution of the CNS. Analyses of Cnidaria and a wide range of bilateria reveal that posterior Hox homeotic gene expression is a universal feature of embryonic development (Holland et al., 2013; Philippidou and Dasen, 2013; Tosches and Arendt, 2013; Arendt et al., 2016). Based upon these observations, we favor the proposed idea that the CNS was formed by merging of the ANS and BNS, and that ANS and BNS may be more or less direct ancestors of the brain and nerve cord, respectively. We further propose that the PcG-Hox program is an ancient system promoting anterior expansion of the CNS.

The anterior CNS expansion process may have come to involve increasingly elaborate daughter cell proliferation modes. Indeed, studies in other vertebrate species have also revealed the existence of proliferating daughter cells in the developing Tel (Dong et al., 2012; Nomura et al., 2013, 2016; McIntosh et al., 2017). However, in gecko lizards dividing daughter cells (basal progenitors) were largely absent (Nomura et al., 2013). In addition, recent studies in zebrafish revealed that although the Tel did display dividing daughter cells, the hindbrain had a higher proportion of these cells (McIntosh et al., 2017). Hence, although there may be a general trend within vertebrates for an A-P gradient of dividing daughter cells, this scenario may have been modified during evolution to promote species-specific and brain region-specific changes in size.

MATERIALS AND METHODS

Fly stocks

The following stocks were obtained from Bloomington *Drosophila* Stock Center: *Df(3L)ED225* (BL#8081; a deletion of *grim*, *rpr*, *skl*, and most of the upstream region of *hid*); dap^{04454} (BL#11377); dap^{Df7867}=*Df(2R)Exel9016* (BL#7867); $E2f^{07172}$ (BL#11717); $E2f^{Df8962}$=*Df(3R)ED6076* (BL#8962); $E2f^{Df7665}$=*Df(3R)ED6186* (BL#7665); $CycE^{AR95}$ (#6637); $CycE^{Df7831}$=*DF(2L)Exel7063* (BL#7831); stg^{4} (BL#2500); stg^{Df7690}=*Df(3R)Exel6212* (BL#7690); esc^{5} (BL#3142); esc^{21} (BL#3623); esc^{Df}=*Df(2L)Exel6030* (BL#7513); *pros-Gal4* on chromosome III (BL#50168). Other stocks used were: *prospero-Gal4* on chromosome III (F. Matsuzaki, Kobe, Japan); *UAS-Ubx* (Merabet et al., 2011) (provided by S. Merabet, Lyon, France); *UAS-Antp* (provided by F. Hirth, King's College, London, UK); *UAS-abd-A* and *UAS-Abd-B* (Monedero Cobeta et al., 2017); *UAS-dap* (Lane et al., 1996) (provided by C. Lehner). Mutants were maintained over *GFP*- or *YFP*-marked balancer chromosomes. *Oregon-R* was used as control. Staging of embryos was performed according to Campos-Ortega and Hartenstein (1985).

Cross scheme for *esc* maternal-zygotic mutants

esc^{5} was crossed to esc^{21}, and from this cross esc^{5}/esc^{21} females were crossed to esc^{Df} males. From this cross *esc* maternal-zygotic mutant embryos (esc^{5}/esc^{Df} or esc^{21}/esc^{Df}) were collected and used in experiments. The same crossing scheme was used to make *esc* maternal-zygotic mutant embryos with PCD background, i.e. esc^{5}/esc^{Df}*;ED225* or esc^{21}/esc^{Df}*; ED225*.

Mouse stocks

The $Eed^{fl/fl}$ allele has loxP sites flanking exons 3-6 (Xie et al., 2014), and was obtained from the Jackson Laboratory Stock Center (stock number #022727). The *Sox1-Cre* line (Takashima et al., 2007) was provided by J. Dias and J. Ericson (Karolinska Institute, Stockholm). Stocks were maintained on a B6:129S1 background. Mice were housed at the Linkoping University animal facility in accordance with best practices, and all procedures involving mice have been approved by the regional animal ethics committee (Dnr 69-14). Pregnant females were sacrificed and embryos dissected between stages E11.5 and E18.5. Primers for genotyping were: Cre1, GCGGTCTGGCAG-TAAAAACTATC; Cre2, GTGAAACAGCATTGCTGTCACTT; Eed1, GGGACGTGCTGACATTTTCT; Eed2, CTTGGGTGGTTTGGCTAAGA.

Immunohistochemistry

Drosophila

Immunohistochemistry (IHC) was performed as previously described (Baumgardt et al., 2009). Primary antibodies were: guinea pig anti-Dap (1:1000) and rat anti-E2f1 (1:100) (Baumgardt et al., 2014); guinea pig anti-Dpn (1:1000) and rat anti-Dpn (1:500) (Ulvklo et al., 2012); rabbit anti-Doc1 (1:1000) (Reim et al., 2003) (provided by M. Frasch); rabbit anti-Tll (1:500) (provided by R. Pflanz, MPI, Göttingen, Germany); rabbit anti-phospho-histone H3-Ser10 (PH3) (1:1000; #06-570, Upstate/Millipore); rabbit monoclonal antibody (mAb) anti-PH3-Ser10 (1:1000; ab177218, Abcam); rat anti-PH3-Ser28 (1:1000; ab10543, Abcam); rat mAb anti-GsbN (1:10) and rat mAb anti-Gsb (1:10) (Buenzow and Holmgren, 1995) (provided by R. Holmgren); mouse mAb anti-Dap (1:500), mAb anti-Ubx (1:10), mAb anti-Abd-A (1:10), mAb vAbd-B (1:10), mAb anti-Antp (1:10) and mAb anti-Pros MR1A (1:10) (Developmental Studies Hybridoma Bank); rabbit anti-Abd-A (1:100) (provided by Maria Capovila, CNRS, Sophia Antipolis, France); rabbit anti-CycE (1:500; #sc-33748; Santa Cruz Biotechnology); rat anti-Stg (1:500) (Bivik et al., 2016); rabbit anti-cleaved caspase-3 (1:300; ab13847, Abcam). Secondary antibodies were AMCA-, FITC-, Rhodamine-RedX- and Cy5/Alexa Fluor647-conjugated donkey antibodies (1:200; Jackson ImmunoResearch Laboratories).

Mouse

Mouse embryos were fixed for 18-36 h in fresh 4% paraformaldehyde (PFA) at 4°C, kept in 30% sucrose at 4°C until saturated, frozen in OCT Tissue Tek (Sakura Finetek) and stored at −80°C. Cryosections (20 and 40 µm thick) were taken for IHC and treated with 4% fresh PFA for 15 min at room temperature, blocked and processed with primary antibodies in PBS with 0.2% Triton X-100 and 4% horse serum overnight at 4°C. Secondary antibodies were conjugated with AMCA, FITC, Rhodamine-RedX or Cy5, and used at 1:200 (Jackson ImmunoResearch). Slides were mounted in Vectashield (Vector Laboratories). Samples were incubated in the EdU detection reaction for 30 min at room temperature between the antibody incubations. IB4 and DAPI were included in the secondary antibody solution. Primary antibodies were: goat anti-Sox2 (1:250; #SC-17320, Santa Cruz Biotechnology); rabbit anti-H3K27me3 (1:500; #9733, Cell Signaling Technology); rat anti-PH3-Ser28 (1:1000; ab10543; Abcam); rabbit anti-CC3 (1:600; #9661, Cell Signaling); rabbit anti-p27-KIP1 (1:250; #ab32034, Abcam); Isolectin GS-IB4-ALEXA647 conjugate ('IB4') (5-20 µg/ml, #I32450, Molecular Probes/Thermo Fisher Scientific); rabbit anti-E2F3 (1:100; ab50917, Abcam); rabbit anti-Cdc25C (1:100; ab84485, Abcam); guinea pig anti-NeuN (1:500; ABN90, Upstate/Merck Millipore); rabbit anti-Tbr1 (1:100; ab31940, Abcam); rabbit anti-Tbr2 (1:100; ab23345, Abcam).

Chicken

Embryos were fixed for 15-18 h in fresh 4% PFA at 4°C, kept in 30% sucrose at 4°C until saturated, frozen in OCT Tissue Tek (Sakura Finetek) and stored at −80°C. Cryosections (40 µm) were taken for IHC and treated with 4% fresh PFA for 15 min at room temperature, blocked and processed with primary antibodies in PBS with 0.2% Triton X-100 and 4% horse serum overnight at 4°C. Secondary antibodies were conjugated with AMCA, FITC, Rhodamine-RedX or Cy5, and used at 1:200 (Jackson ImmunoResearch). Slides were mounted in Vectashield (Vector Laboratories). Primary antibodies were: goat anti-Sox2 (1:250; #SC-17320, Santa Cruz Biotechnology); mouse anti-Sox2 (1:100; ab171380, Abcam); goat anti-GFP (1:1000; ab6673, Abcam); chicken anti-GFP (1:1000; ab13970, Abcam); rabbit mAb anti-PH3-Ser10 (1:1000; ab177218, Abcam); mouse anti-Myc (1:1000; #05-724; Upstate/Millipore).

Development (2018) 145, dev160747. doi:10.1242/dev.160747

EdU labeling

Drosophila embryos at St13-14 were dechorionated in 4% sodium hypochlorite, and the vitelline membrane was manually removed in Schneider medium. Devitellinated embryos were pulsed for 40 min with EdU solution (0.5 mM EdU, 0.1 mM KCl, Schneider medium) at 25°C (Molecular Probes Click-iT Plus EdU AlexaFluor 647 Imaging Kit). The CNS was dissected on poly-L-lysine-coated slides and fixed with 4% PFA for 20 min. The Click-iT Plus reaction was carried out as per manufacturer's instructions. Slides were immunostained as previously described (Bahrampour et al., 2017). Female mice at a specific time of pregnancy (see main text) were administered 1 ml EdU intraperitoneally (10 µg/ml), 12-24 h before sacrifice. EdU staining was performed as described for *Drosophila* immunohistochemistry.

Confocal imaging and data acquisition

Zeiss LSM700 or Zeiss LSM800 confocal microscopes were used for fluorescent images. Confocal stacks were merged using LSM software or Fiji software (Schindelin et al., 2012). Images and graphs were compiled in Adobe Illustrator.

Chick electroporation

The sequences coding for Hoxb9 and Hoxb13 were codon optimized for chick expression (Genscript). *Eco*RI site and consensus start codon (Kozak, 1984) were added to the 5′ end. To the 3′ end, stop codons (amb, och, opa) followed by an *Xba*I site were added (see supplementary Materials and Methods for DNA sequences). DNA was generated by gene synthesis (Genscript), and cloned into plasmid pCAGGS as *Eco*RI/*Xba*I fragments. pCAGGS-GFP (kindly provided by Maria Bergsland, Karolinska Institute, Stockholm, Sweden) was co-injected as reference.

White leghorn eggs were supplied by SwedFarm AB (Linghem, Sweden). Eggs were incubated at 37.8°C, 45% humidity for 2 days prior to injection of plasmid. Plasmids (1 µg/µl+0.05% Phenol Red) were injected into the lumen of the anterior neural tube using pneumatic microinjection pump (Picospritzer II, Parker Hannifin). Electroporation electrodes (0.9 mm diameter with an exposed length of 4 mm) were placed on the vitelline membrane, spanning the brain, at a distance of 8 mm apart. A small volume of Leibovitz's L15 medium (Gibco) was added between the electrodes. Then a square pulse of 25 V, 50 ms followed by 950 ms rest phase was charged three times. This procedure was repeated two or three times for each embryo. Pulses were generated by an ECM 830 Electro Square Porator from BTX. After electroporation, L15 medium with antibiotics and antimycotics (1% solution containing 100 units/ml penicillin, 100 µg/ml streptomycin and 0.25 µg/ml amphotericin B) was added and the eggs were patched up using adhesive tape (Scotch). Eggs was kept in the incubator for 24 h (37.8°C, 45% humidity) before harvesting the embryos. Immunohistochemistry was performed as described above.

Quantification of proliferation and cell numbers

Drosophila: Global quantification of proliferation and estimation of Type I division mode

Embryos were collected at 100-min intervals (see graphs for precise time points, i.e. embryonic stages) and mitotic NBs and daughter cells were counted within each segment. Occasionally, some mitotic cells did not match the typical NB or daughter cell profile, and were not included in the analysis. An ImageJ macro (automated series of ImageJ commands) combined with user based interface for region of interest selection was designed and used for the quantification with Fiji software. NB and daughter cell comparative proliferation percentages in B1-B2, T2-T3 and A8-A10 were calculated by dividing the numbers for mitotic NBs and daughter cells at different stages in these three regions by the numbers of total NBs generated in each region, i.e. B1-B2=101 NBs, T2-T3=128 NBs, A8-A10=130 NBs (data for T2-T3 and A8-A10 was taken from our previous study; Monedero Cobeta et al., 2017).

Drosophila: Quantification of total cell numbers

Embryos were fixed for 20 min in 4% PFA, followed by permeabilization with 99% methanol for 5 min. After fixation, immunostaining was performed as previously described (Baumgardt et al., 2014). Embryos were mounted in Vectashield with 4′,6-diamidino-2-phenylindole (DAPI) (H-1200, Vector Laboratories). A semi-automated macro (ImageJ macro language-based) was designed and used for quantification of the volume of each segment with Fiji software. The same software was used to count manually the number of cells and volumes of areas of brain, thorax and abdomen in different genotypes, thereby allowing estimation of average single cell volume. Total number of cells was estimated as the ratio of the total volume of the segment to the average single cell volume. Because there are fewer NBs in B1-B2 (101) than in either T2-T3 (128) or A8-A10 (130), total cell numbers obtained for T2-T3 and A8-A10 in control and *ED225* mutants were adjusted to the total NBs in B1-B2. This adjustment was achieved by multiplying total cell numbers in T2-T3 and A8-A10 by their respective quotients of $B1\text{-}B2_{NBs}/T2\text{-}T3_{NBs}=0.79$ and $B1\text{-}B2_{NBs}/A8\text{-}A10_{NBs}=0.78$. The adjusted values were then plotted against total cell numbers in B1-B2 for comparison (Fig. 1H).

Drosophila: Quantification of lineage size

The total number of cells was divided by the known number of NBs, which delaminate in each of the three regions studied, i.e. B1-B2=101 [93 based on Urbach et al. (2003); eight based upon Walsh and Doe (2017)], T2-T3=128 and A8-A10=130.

Chicken: Quantification of proliferation

$PH3^+$ $Sox2^+$ cells of Tel in horizontal sections of day 3 chicken embryos were counted along the stretch of cells that had incorporated and expressed the electroporated plasmids (GFP^+), using Fiji software. Values were normalized for the lumen area (length and section thickness; mm^2). For the negative control, a proportionate length of the telencephalic lumen on the non-electroporated (−) side of the brain was selected and analyzed.

Mouse: Quantification of proliferation

Mouse PH3 and Sox2 staining was quantified using Fiji software (Schindelin et al., 2012, 2015). $PH3^+$ cells were counted in Tel in a volume defined by a selection 200 µm along the edge of the lateral ventricles of horizontal sections and out to the plate (rectangular selection with sides equal to the visible depth of the Tel, and excluding non-CNS tissue; see box in Fig. 6E for an example), and in SC for a volume defined within its anatomical perimeter. 3D reconstruction and volume quantification of DAPI and Sox2 signal in the aforementioned regions was calculated using the 3DViewer Fiji plugin, taking into account a binary mask value of 255 (Schmid et al., 2010).

Mouse: Quantification of mitotic cell distribution

The distance (µm) of $PH3^+$ cells to the lumen in Tel and SC sections of control and *Eed-cKO* was measured using Fiji software. Based on positional distribution of $PH3^+$ cells in relation to the lumen, we binned the $PH3^+$ cells which were more than 20 µm distant from the lumen as mitotic daughter cells, and normalized this value in every measured section for lumen area (length and section thickness mm^2) along which the quantification was performed.

Mouse: Generation of cortical staining profiles

Cortical staining profiles were created by first obtaining plot profiles in ImageJ of five to ten bands (~40 µm wide, orthogonal to the lumen, two to four scans) per sum-projected confocal stack for the channel of interest. The intensity data were normalized to the maximum intensity percentage per individual profile. A high-order polynomial fit was used to approximate the staining profile (y) across the tissue thickness (x) using GraphPad Prism. The tabular data of the function describing each profile was grouped according to age and genotype for each tissue thickness value, and scaled according to the measured thickness of the tissue. The mean plot for each channel (Sox2, Tbr2, Tbr1, CC3, p27) was combined as one graph per group.

Statistical analysis

Shapiro–Wilk normality test, two-tailed Student's *t*-test, independent samples Kruskal–Wallis test, Bonferroni or Benjamini–Hochberg

Development (2018) 145, dev160747. doi:10.1242/dev.160747

correction for multiple test, two-tailed Mann–Whitney *U*-test, one-way ANOVA and Levene test of homogeneity of variance were performed using SPSS v.24 (IBM; for specific statistical test used, see text). Microsoft Excel 2010 and GraphPad Prism 6 were used for data compilation and graphical representation.

Fluorescence intensity measurements

Drosophila

Embryos of different genotypes and/or stages were dissected on the same slide to ensure identical staining conditions. The integrated density (mean pixel intensity×area occupied by the signal) of individual cells was measured using Fiji software on single 1-µm-thick confocal layers encompassing the center of the cells. Mitotic ($PH3^+$ Dpn^+) and non-mitotic (Dpn^+) NBs were measured. When more than one slide was needed to achieve an adequate number of replicates, the mean pixel intensity (histogram mean) of the segment signal in control embryos of the same stage was used to normalize values between slides, to allow for comparisons between multiple genotypes or stages.

Mouse

Embryos were frozen in OCT Tissue Tek (Sakura Finetek) in pairs (control and *Eed-cKO*) to ensure identical conditions. Cryosections (40 µm thick) were stained on the same slide to ensure identical staining conditions. The integrated density (mean pixel intensity×area occupied by the signal) of Cdc25C and E2F3 signals (32-bit sum intensity *z* projection) was measured in the $Sox2^+$ area and in $Sox2^+$ area within 20 µm from the lumen border, using Fiji software. For measurement of mitotic progenitors, mitotic progenitor ($PH3^+$ $Sox2^+$) cells within 20 µm of the lumen were outlined and measured. Integrated density of individual cells was measured using Fiji software on single 3-µm-thick confocal layers encompassing the center of the cells.

RNA-seq

Drosophila

St14-15 embryos were collected and RNA was isolated from whole embryos (Qiagen RNeasy Mini kit, 74104). RNA sequencing library preparation used the NEBNext Ultra RNA Library Prep Kit for Illumina following the manufacturer's recommendations (NEB). The sequencing libraries were multiplexed and clustered. Samples were sequenced on Illumina HiSeq 2500 using a 2×150 Paired End (PE) configuration with a depth of ∼50 million reads (GeneWiz). FASTQ-files were aligned to *Drosophila melanogaster* Release 6 plus ISO1 MT reference genomes using QSeq (DNASTAR LaserGene 14) and gene-level reads were normalized as RPKM. Genes of interest were defined prior to analysis and presented in heat maps.

Mouse

E15.5 mouse embryos were dissected to extricate the anterior CNS. The forebrain was resected by a coronal cut posterior to the telencephalon, but anterior to the pretectum. Samples were stored at −80°C until RNA isolation (Qiagen RNeasy Mini kit, 74104). RNA sequencing library preparation used the NEBNext Ultra RNA Library Prep Kit for Illumina following the manufacturer's recommendations (NEB). The sequencing libraries were multiplexed and clustered. Samples were sequenced on Illumina HiSeq 2500 using a 1×50 bp Single Read (SR) configuration with a depth of ∼50 million reads (GeneWiz). FASTQ-files were aligned to Mouse mm9 reference genomes using QSeq (DNASTAR LaserGene 14) and gene-level reads were normalized as RPKM. Genes of interest were defined prior to analysis and presented in heat maps.

Acknowledgements

We are grateful to Laure Bally-Cuif, Magdalena Götz, Maria Bergsland, José Dias, Johan Ericson, Mattias Mannervik, Fumio Matsuzaki, Frank Hirth, Samir Merabet, Maria Capovila, Christian Lehner, Robert Holmgren, Manfred Frasch, Ralf Pflanz, the Developmental Studies Hybridoma Bank at the University of Iowa, The Jackson Laboratory mouse stock center, and the Bloomington Stock Center for sharing reagents and advice. We thank José Dias, Don van Meyel and Douglas W. Allan for critically reading the manuscript. Helen Ekman and Carolin Jonsson provided excellent technical assistance.

Competing interests

The authors declare no competing or financial interests.

Author contributions

Conceptualization: B.Y.S., S.T.; Methodology: B.Y.S., I.M.C., J.R., S.T.; Software: I.M.C., J.R.; Formal analysis: B.Y.S., I.M.C., J.R., S.B., J.R.C., A.S.; Investigation: B.Y.S., I.M.C., J.R., S.B., J.R.C., A.S., S.T.; Resources: S.T.; Data curation: B.Y.S., I.M.C., J.R., S.B., J.R.C.; Writing - original draft: B.Y.S., I.M.C., J.R., S.T.; Supervision: S.T.; Project administration: S.T.; Funding acquisition: S.T.

Funding

Funding was provided by the Swedish Research Council (Vetenskapsrådet; 621-2013-5258), the Knut and Alice Wallenberg Foundation (Knut och Alice Wallenbergs Stiftelse; KAW2011.0165 and KAW2012.0101) and the Swedish Cancer Foundation (Cancerfonden; 140780 and 150663) to S.T.

Data availability

RNA-seq data have been deposited in Gene Expression Omnibus under accession numbers GSE111324 (*Drosophila*) and GSE111232 (mouse).

Supplementary information

Supplementary information available online at
http://dev.biologists.org/lookup/doi/10.1242/dev.160747.supplemental

References

Arendt, D., Tosches, M. A. and Marlow, H. (2016). From nerve net to nerve ring, nerve cord and brain–evolution of the nervous system. *Nat. Rev. Neurosci.* **17**, 61-72.

Bahrampour, S., Gunnar, E., Jonsson, C., Ekman, H. and Thor, S. (2017). Neural lineage progression controlled by a temporal proliferation program. *Dev. Cell* **43**, 332-348.e4.

Baumgardt, M., Karlsson, D., Terriente, J., Díaz-Benjumea, F. J. and Thor, S. (2009). Neuronal subtype specification within a lineage by opposing temporal feed-forward loops. *Cell* **139**, 969-982.

Baumgardt, M., Karlsson, D., Salmani, B. Y., Bivik, C., MacDonald, R. B., Gunnar, E. and Thor, S. (2014). Global programmed switch in neural daughter cell proliferation mode triggered by a temporal gene cascade. *Dev. Cell* **30**, 192-208.

Bello, B. C., Izergina, N., Caussinus, E. and Reichert, H. (2008). Amplification of neural stem cell proliferation by intermediate progenitor cells in Drosophila brain development. *Neural Dev.* **3**, 5.

Bergmann, O., Spalding, K. L. and Frisén, J. (2015). Adult neurogenesis in humans. *Cold Spring Harb. Perspect. Biol.* **7**, a018994.

Bertet, C., Li, X., Erclik, T., Cavey, M., Wells, B. and Desplan, C. (2014). Temporal patterning of neuroblasts controls Notch-mediated cell survival through regulation of Hid or Reaper. *Cell* **158**, 1173-1186.

Betizeau, M., Cortay, V., Patti, D., Pfister, S., Gautier, E., Bellemin-Ménard, A., Afanassieff, M., Huissoud, C., Douglas, R. J., Kennedy, H. et al. (2013). Precursor diversity and complexity of lineage relationships in the outer subventricular zone of the primate. *Neuron* **80**, 442-457.

Bivik, C., Bahrampour, S., Ulvklo, C., Nilsson, P., Angel, A., Fransson, F., Lundin, E., Renhorn, J. and Thor, S. (2015). Novel genes involved in controlling specification of Drosophila FMRFamide neuropeptide cells. *Genetics* **200**, 1229-1244.

Bivik, C., MacDonald, R. B., Gunnar, E., Mazouni, K., Schweisguth, F. and Thor, S. (2016). Control of neural daughter cell proliferation by multi-level Notch/Su(H)/E(spl)-HLH signaling. *PLoS Genet.* **12**, e1005984.

Boone, J. Q. and Doe, C. Q. (2008). Identification of Drosophila type II neuroblast lineages containing transit amplifying ganglion mother cells. *Dev. Neurobiol.* **68**, 1185-1195.

Bowman, S. K., Rolland, V., Betschinger, J., Kinsey, K. A., Emery, G. and Knoblich, J. A. (2008). The tumor suppressors Brat and Numb regulate transit-amplifying neuroblast lineages in Drosophila. *Dev. Cell* **14**, 535-546.

Buenzow, D. E. and Holmgren, R. (1995). Expression of the Drosophila gooseberry locus defines a subset of neuroblast lineages in the central nervous system. *Dev. Biol.* **170**, 338-349.

Campos-Ortega, J. A. and Hartenstein, V. (1985). *The Embryonic Development of Drosophila melanogaster*. New York: Springer-Verlag.

Cappella, P., Gasparri, F., Pulici, M. and Moll, J. (2008). A novel method based on click chemistry, which overcomes limitations of cell cycle analysis by classical determination of BrdU incorporation, allowing multiplex antibody staining. *Cytometry A* **73A**, 626-636.

Caviness, V. S., Jr, Takahashi, T. and Nowakowski, R. S. (1995). Numbers, time and neocortical neuronogenesis: a general developmental and evolutionary model. *Trends Neurosci.* **18**, 379-383.

Doe, C. Q. (1992). Molecular markers for identified neuroblasts and ganglion mother cells in the Drosophila central nervous system. *Development* **116**, 855-863.

Doe, C. Q. (2008). Neural stem cells: balancing self-renewal with differentiation. *Development* **135**, 1575-1587.
Dong, Z., Yang, N., Yeo, S.-Y., Chitnis, A. and Guo, S. (2012). Intralineage directional Notch signaling regulates self-renewal and differentiation of asymmetrically dividing radial glia. *Neuron* **74**, 65-78.
Dumesic, P. A., Homer, C. M., Moresco, J. J., Pack, L. R., Shanle, E. K., Coyle, S. M., Strahl, B. D., Fujimori, D. G., Yates, J. R., III and Madhani, H. D. (2015). Product binding enforces the genomic specificity of a yeast polycomb repressive complex. *Cell* **160**, 204-218.
Economides, K. D., Zeltser, L. and Capecchi, M. R. (2003). Hoxb13 mutations cause overgrowth of caudal spinal cord and tail vertebrae. *Dev. Biol.* **256**, 317-330.
Englund, C., Fink, A., Lau, C., Pham, D., Daza, R. A., Bulfone, A., Kowalczyk, T. and Hevner, R. F. (2005). Pax6, Tbr2, and Tbr1 are expressed sequentially by radial glia, intermediate progenitor cells, and postmitotic neurons in developing neocortex. *J. Neurosci.* **25**, 247-251.
Fasano, C. A., Phoenix, T. N., Kokovay, E., Lowry, N., Elkabetz, Y., Dimos, J. T., Lemischka, I. R., Studer, L. and Temple, S. (2009). Bmi-1 cooperates with Foxg1 to maintain neural stem cell self-renewal in the forebrain. *Genes Dev.* **23**, 561-574.
Feng, X., Juan, A. H., Wang, H. A., Ko, K. D., Zare, H. and Sartorelli, V. (2016). Polycomb Ezh2 controls the fate of GABAergic neurons in the embryonic cerebellum. *Development* **143**, 1971-1980.
Fish, J. L., Dehay, C., Kennedy, H. and Huttner, W. B. (2008). Making bigger brains-the evolution of neural-progenitor-cell division. *J. Cell Sci.* **121**, 2783-2793.
Franco, S. J. and Müller, U. (2013). Shaping our minds: stem and progenitor cell diversity in the mammalian neocortex. *Neuron* **77**, 19-34.
Gage, F. H. and Temple, S. (2013). Neural stem cells: generating and regenerating the brain. *Neuron* **80**, 588-601.
Garcia-Fernàndez, J. (2005). The genesis and evolution of homeobox gene clusters. *Nat. Rev. Genet.* **6**, 881-892.
Götz, M. and Huttner, W. B. (2005). The cell biology of neurogenesis. *Nat. Rev. Mol. Cell Biol.* **6**, 777-788.
Hartenstein, V., Rudloff, E. and Campos-Ortega, J. A. (1987). The pattern of proliferation of the neuroblasts in the wild-type embryo of Drosophila melanogaster. *Roux Arch. dev. Biol.* **196**, 473-485.
Hirth, F., Hartmann, B. and Reichert, H. (1998). Homeotic gene action in embryonic brain development of Drosophila. *Development* **125**, 1579-1589.
Holland, N. D. (2003). Early central nervous system evolution: an era of skin brains? *Nat. Rev. Neurosci.* **4**, 617-627.
Holland, P. W. H. (2013). Evolution of homeobox genes. *Wiley Interdiscip. Rev. Dev. Biol.* **2**, 31-45.
Holland, L. Z., Carvalho, J. E., Escriva, H., Laudet, V., Schubert, M., Shimeld, S. M. and Yu, J.-K. (2013). Evolution of bilaterian central nervous systems: a single origin? *Evodevo* **4**, 27.
Huang, J., Chen, J., Wang, W., Wei, Y.-Y., Cai, G.-H., Tamamaki, N., Li, Y.-Q. and Wu, S.-X. (2013). Birthdate study of GABAergic neurons in the lumbar spinal cord of the glutamic acid decarboxylase 67-green fluorescent protein knock-in mouse. *Front. Neuroanat.* **7**, 42.
Isono, K., Fujimura, Y., Shinga, J., Yamaki, M., O. Wang, J., Takihara, Y., Murahashi, Y., Takada, Y., Mizutani-Koseki, Y. and Koseki, H. (2005). Mammalian polyhomeotic homologues Phc2 and Phc1 act in synergy to mediate polycomb repression of Hox genes. *Mol. Cell. Biol.* **25**, 6694-6706.
Jamieson, K., Rountree, M. R., Lewis, Z. A., Stajich, J. E. and Selker, E. U. (2013). Regional control of histone H3 lysine 27 methylation in Neurospora. *Proc. Natl. Acad. Sci. USA* **110**, 6027-6032.
Jékely, G., Paps, J. and Nielsen, C. (2015). The phylogenetic position of ctenophores and the origin(s) of nervous systems. *Evodevo* **6**, 1.
Jung, H. and Dasen, J. S. (2015). Evolution of patterning systems and circuit elements for locomotion. *Dev. Cell* **32**, 408-422.
Karcavich, R. and Doe, C. Q. (2005). Drosophila neuroblast 7-3 cell lineage: a model system for studying programmed cell death, Notch/Numb signaling, and sequential specification of ganglion mother cell identity. *J. Comp. Neurol.* **481**, 240-251.
Karlsson, D., Baumgardt, M. and Thor, S. (2010). Segment-specific neuronal subtype specification by the integration of anteroposterior and temporal cues. *PLoS Biol.* **8**, e1000368.
Kicheva, A., Bollenbach, T., Ribeiro, A., Valle, H. P., Lovell-Badge, R., Episkopou, V. and Briscoe, J. (2014). Coordination of progenitor specification and growth in mouse and chick spinal cord. *Science* **345**, 1254927.
Kozak, M. (1984). Compilation and analysis of sequences upstream from the translational start site in eukaryotic mRNAs. *Nucleic Acids Res.* **12**, 857-872.
Kriegstein, A., Noctor, S. and Martínez-Cerdeño, V. (2006). Patterns of neural stem and progenitor cell division may underlie evolutionary cortical expansion. *Nat. Rev. Neurosci.* **7**, 883-890.
Kurusu, M., Maruyama, Y., Adachi, Y., Okabe, M., Suzuki, E. and Furukubo-Tokunaga, K. (2009). A conserved nuclear receptor, Tailless, is required for efficient proliferation and prolonged maintenance of mushroom body progenitors in the Drosophila brain. *Dev. Biol.* **326**, 224-236.
Lane, M. E., Sauer, K., Wallace, K., Jan, Y. N., Lehner, C. F. and Vaessin, H. (1996). Dacapo, a cyclin-dependent kinase inhibitor, stops cell proliferation during Drosophila development. *Cell* **87**, 1225-1235.
Leber, S. M. and Sanes, J. R. (1995). Migratory paths of neurons and glia in the embryonic chick spinal cord. *J. Neurosci.* **15**, 1236-1248.
Li, X., Isono, K., Yamada, D., Endo, T. A., Endoh, M., Shinga, J., Mizutani-Koseki, Y., Otte, A. P., Casanova, M., Kitamura, H. et al. (2011). Mammalian polycomb-like Pcl2/Mtf2 is a novel regulatory component of PRC2 that can differentially modulate polycomb activity both at the Hox gene cluster and at Cdkn2a genes. *Mol. Cell. Biol.* **31**, 351-364.
Lui, J. H., Hansen, D. V. and Kriegstein, A. R. (2011). Development and evolution of the human neocortex. *Cell* **146**, 18-36.
Martín-Durán, J. M., Pang, K., Borve, A., Le, H. S., Furu, A., Cannon, J. T., Jondelius, U. and Hejnol, A. (2017). Convergent evolution of bilaterian nerve cords. *Nature* **553**, 45-50.
Martínez-Cerdeño, V. and Noctor, S. C. (2016). Cortical evolution 2015: discussion of neural progenitor cell nomenclature. *J. Comp. Neurol.* **524**, 704-709.
McIntosh, R., Norris, J., Clarke, J. D. and Alexandre, P. (2017). Spatial distribution and characterization of non-apical progenitors in the zebrafish embryo central nervous system. *Open Biol.* **7**, 160312.
Merabet, S., Litim-Mecheri, I., Karlsson, D., Dixit, R., Saadaoui, M., Monier, B., Brun, C., Thor, S., Vijayraghavan, K., Perrin, L. et al. (2011). Insights into Hox protein function from a large scale combinatorial analysis of protein domains. *PLoS Genet.* **7**, e1002302.
Monedero Cobeta, I., Salmani, B. Y. and Thor, S. (2017). Anterior-posterior gradient in neural stem and daughter cell proliferation governed by spatial and temporal Hox control. *Curr. Biol.* **27**, 1161-1172.
Müller, J. and Verrijzer, P. (2009). Biochemical mechanisms of gene regulation by polycomb group protein complexes. *Curr. Opin. Genet. Dev.* **19**, 150-158.
Nielsen, C. (2012). How to make a protostome. *Invertebr. Systemat.* **26**, 25-40.
Nielsen, C. (2015). Larval nervous systems: true larval and precocious adult. *J. Exp. Biol.* **218**, 629-636.
Nomura, T., Gotoh, H. and Ono, K. (2013). Changes in the regulation of cortical neurogenesis contribute to encephalization during amniote brain evolution. *Nat. Commun.* **4**, 2206.
Nomura, T., Ohtaka-Maruyama, C., Yamashita, W., Wakamatsu, Y., Murakami, Y., Calegari, F., Suzuki, K., Gotoh, H. and Ono, K. (2016). The evolution of basal progenitors in the developing non-mammalian brain. *Development* **143**, 66-74.
Philippidou, P. and Dasen, J. S. (2013). Hox genes: choreographers in neural development, architects of circuit organization. *Neuron* **80**, 12-34.
Piunti, A. and Shilatifard, A. (2016). Epigenetic balance of gene expression by Polycomb and COMPASS families. *Science* **352**, aad9780.
Reim, I., Lee, H. H. and Frasch, M. (2003). The T-box-encoding Dorsocross genes function in amnioserosa development and the patterning of the dorsolateral germ band downstream of Dpp. *Development* **130**, 3187-3204.
Schindelin, J., Arganda-Carreras, I., Frise, E., Kaynig, V., Longair, M., Pietzsch, T., Preibisch, S., Rueden, C., Saalfeld, S., Schmid, B. et al. (2012). Fiji: an open-source platform for biological-image analysis. *Nat. Methods* **9**, 676-682.
Schindelin, J., Rueden, C. T., Hiner, M. C. and Eliceiri, K. W. (2015). The ImageJ ecosystem: an open platform for biomedical image analysis. *Mol. Reprod. Dev.* **82**, 518-529.
Schmid, B., Schindelin, J., Cardona, A., Longair, M. and Heisenberg, M. (2010). A high-level 3D visualization API for Java and ImageJ. *BMC Bioinformatics* **11**, 274.
Schumacher, A., Faust, C. and Magnuson, T. (1996). Positional cloning of a global regulator of anterior-posterior patterning in mice. *Nature* **384**, 648.
Steffen, P. A. and Ringrose, L. (2014). What are memories made of? How Polycomb and Trithorax proteins mediate epigenetic memory. *Nat. Rev. Mol. Cell Biol.* **15**, 340-356.
Struhl, G. (1983). Role of the esc+ gene product in ensuring the selective expression of segment-specific homeotic genes in Drosophila. *J. Embryol. Exp. Morphol.* **76**, 297-331.
Struhl, G. and Akam, M. (1985). Altered distributions of Ultrabithorax transcripts in extra sex combs mutant embryos of Drosophila. *EMBO J.* **4**, 3259-3264.
Stubbs, D., DeProto, J., Nie, K., Englund, C., Mahmud, I., Hevner, R. and Molnar, Z. (2009). Neurovascular congruence during cerebral cortical development. *Cereb. Cortex* **19** Suppl. 1, i32-i41.
Suzuki, M., Mizutani-Koseki, Y., Fujimura, Y., Miyagishima, H., Kaneko, T., Takada, Y., Akasaka, T., Tanzawa, H., Takihara, Y., Nakano, M. et al. (2002). Involvement of the Polycomb-group gene Ring1B in the specification of the anterior-posterior axis in mice. *Development* **129**, 4171-4183.
Takashima, Y., Era, T., Nakao, K., Kondo, S., Kasuga, M., Smith, A. G. and Nishikawa, S.-I. (2007). Neuroepithelial cells supply an initial transient wave of MSC differentiation. *Cell* **129**, 1377-1388.
Technau, G. M., Rogulja-Ortmann, A., Berger, C., Birkholz, O. and Rickert, C. (2014). Composition of a Neuromere and its segmental diversification under the control of Hox genes in the embryonic CNS of Drosophila. *J. Neurogenet.*, **28**, 171-180.
Tosches, M. A. and Arendt, D. (2013). The bilaterian forebrain: an evolutionary chimaera. *Curr. Opin. Neurobiol.* **23**, 1080-1089.

Ulvklo, C., Macdonald, R., Bivik, C., Baumgardt, M., Karlsson, D. and Thor, S. (2012). Control of neuronal cell fate and number by integration of distinct daughter cell proliferation modes with temporal progression. *Development* **139**, 678-689.

Urbach, R., Schnabel, R. and Technau, G. M. (2003). The pattern of neuroblast formation, mitotic domains and proneural gene expression during early brain development in Drosophila. *Development* **130**, 3589-3606.

Urbach, R., Jussen, D. and Technau, G. M. (2016). Gene expression profiles uncover individual identities of gnathal neuroblasts and serial homologies in the embryonic CNS of Drosophila. *Development* **143**, 1290-1301.

Walsh, K. T. and Doe, C. Q. (2017). Drosophila embryonic type II neuroblasts: origin, temporal patterning, and contribution to the adult central complex. *Development* **144**, 4552-4562.

Wang, J., Mager, J., Schnedier, E. and Magnuson, T. (2002). The mouse PcG gene eed is required for Hox gene repression and extraembryonic development. *Mamm. Genome* **13**, 493-503.

Xie, H., Xu, J., Hsu, J. H., Nguyen, M., Fujiwara, Y., Peng, C. and Orkin, S. H. (2014). Polycomb repressive complex 2 regulates normal hematopoietic stem cell function in a developmental-stage-specific manner. *Cell Stem Cell* **14**, 68-80.

Zemke, M., Draganova, K., Klug, A., Schöler, A., Zurkirchen, L., Gay, M. H.-P., Cheng, P., Koseki, H., Valenta, T., Schübeler, D. et al. (2015). Loss of Ezh2 promotes a midbrain-to-forebrain identity switch by direct gene derepression and Wnt-dependent regulation. *BMC Biol.* **13**, 103.

Zencak, D., Lingbeek, M., Kostic, C., Tekaya, M., Tanger, E., Hornfeld, D., Jaquet, M., Munier, F. L., Schorderet, D. F., van Lohuizen, M. et al. (2005). Bmi1 loss produces an increase in astroglial cells and a decrease in neural stem cell population and proliferation. *J. Neurosci.* **25**, 5774-5783.

Supplemental Table 1, related to Fig. 1

Estimated average cell volumes per genotype and region at St16+200 min

	B1-B2 average cell volume (μm^3)	SD	T2-T3 average cell volume (μm^3)	SD	A8-A10 average cell volume (μm^3)	SD
Control	**70.30**	**5.41**	**72.83**	**12.76**	**68.82**	**16.55**
ED225	**48.99 ****	**9.19**	**48.99 ****	**5.55**	**54.32 ***	**6.96**

The values for average cell volume in B1-B2, T2-T3 and A8-A10 were used to estimate total cell numbers in these three regions in control and *ED225* mutant embryos (Fig. 1h). The average cell volume is calculated as the ratio of the volume of restricted DAPI signal to the number of cells, manually counted in that region. Independent measurements were done for control and *ED225* mutant embryos in the specified regions of the brain, thorax and abdomen. No significant differences were observed between average cell volumes in the three regions for either genotypes (one-way ANOVA; control; $p \geq 0.9$, *ED225*; $p \geq 0.59$, $n \geq 5$ embryos per genotype and region). In all three regions, the average cell volumes for *ED225* mutants were significantly lower than those of control embryos (two-tailed Student's T-test, * $p \leq 0.05$, ** $p \leq 0.01$; SD= standard deviation; $n \geq 5$ embryos per genotype and region).

Supplemental Table 2, related to Fig. 3

Estimated average cell volumes per genotype in B1-B2 at St16+200 min

	B1-B2 average cell volume (μm^3)	SD
prosG4,ED225	**71.10**	**12.82**
pros>BX-C,ED225	**82.69**	**14.16**

The average cell volume of each genotype was used to estimate total cell numbers in B1-B2 (Fig. 3m). The average cell volume is calculated as the ratio of the volume of restricted DAPI signal to the number of cells, manually counted in that region. Independent measurements were done for *prosG4,ED225* and *pros>BX-C,ED225* embryos in B1-B2 hemi-segments of the brain. No significant difference was observed between average cell volumes of the two genotypes (two-tailed Student's T-test, $p \geq 0.07$; SD= standard deviation; $n \geq 5$ embryos per genotype).

Supplemental Table 3, related to Fig. 4

Estimated average cell volumes per genotype and region at St16+200 min

	B1-B2 average cell volume (μm^3)	SD	A8-A10 average cell volume (μm^3)	SD
ED225	**48.99**	**9.19**	**54.32**	**6.96**
esc;ED225	**89.65 *****	**17.48**	**66.49 ***	**15.56**

The values for average cell volume in B1-B2 and A8-A10 were used to estimate total cell numbers in these regions in *ED225* and *esc;ED225* mutant embryos (Fig. 4v). The average cell volume is calculated as the ratio of the volume of restricted DAPI signal to the number of cells, manually counted in that region. Independent measurements were done for *ED225* and *esc;ED225* mutant embryos in the specified regions of the brain and abdomen. In both regions, the average cell volumes for *ED225* mutants were significantly lower than those of *esc;ED225* embryos (two-tailed Student's T-test, * $p \leq 0.05$, ** $p \leq 0.01$; *** $p \leq 0.001$; SD= standard deviation; $n \geq 5$ embryos per genotype and region).

Supplemental Figures

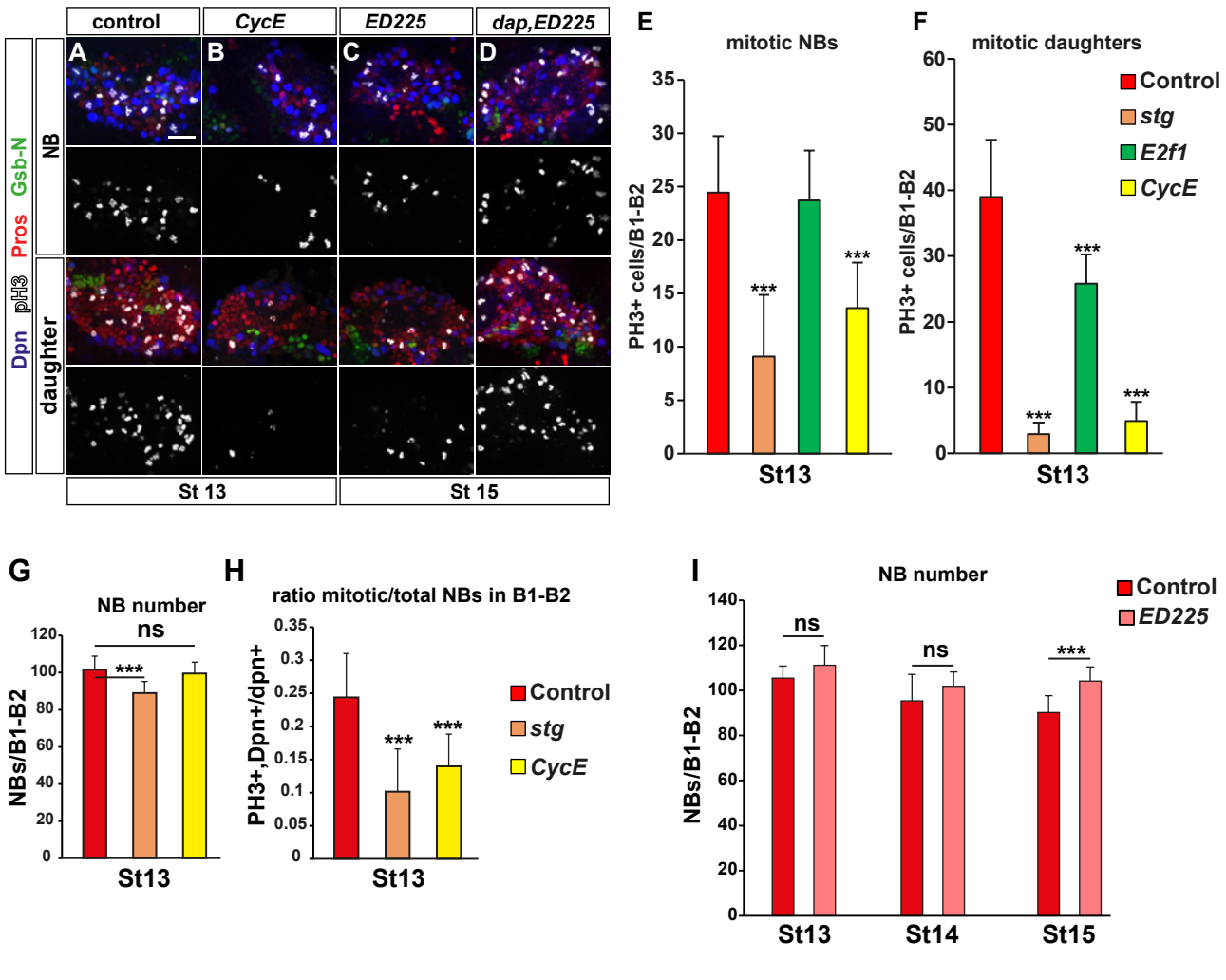

Figure S1.

The brain depends on the same four key cell cycle genes as the nerve cord.

(A-D) z-Projections of brain lobes showing mitotic NBs (upper panels) and daughters (lower panels), at St13 in control, *CycE*, *ED225* and *dap;ED225* mutants, at St15 (scale bar, 20µm). (E-F) Quantification of mitotic NBs and daughters in B1-B2, at St13 in control, *stg*, *E2f1* and *CycE* mutants. (G) Quantification of total NB numbers in B1-B2 at St13 in control, *stg* and *CycE* mutants. (H) Ratio of mitotic to total NBs in control, *stg* and *CycE* mutants in B1-B2 at St13. (I) Quantification of total NB numbers in B1-B2 at stages 13,14 and 15 in control and *ED225*. (J-K) Quantification of mitotic NBs and daughters in B1-B2, at St15 in control, *dap*, *ED225* and *dap;ED225* (Student's t test; SD; n≥10 embryos per genotype).

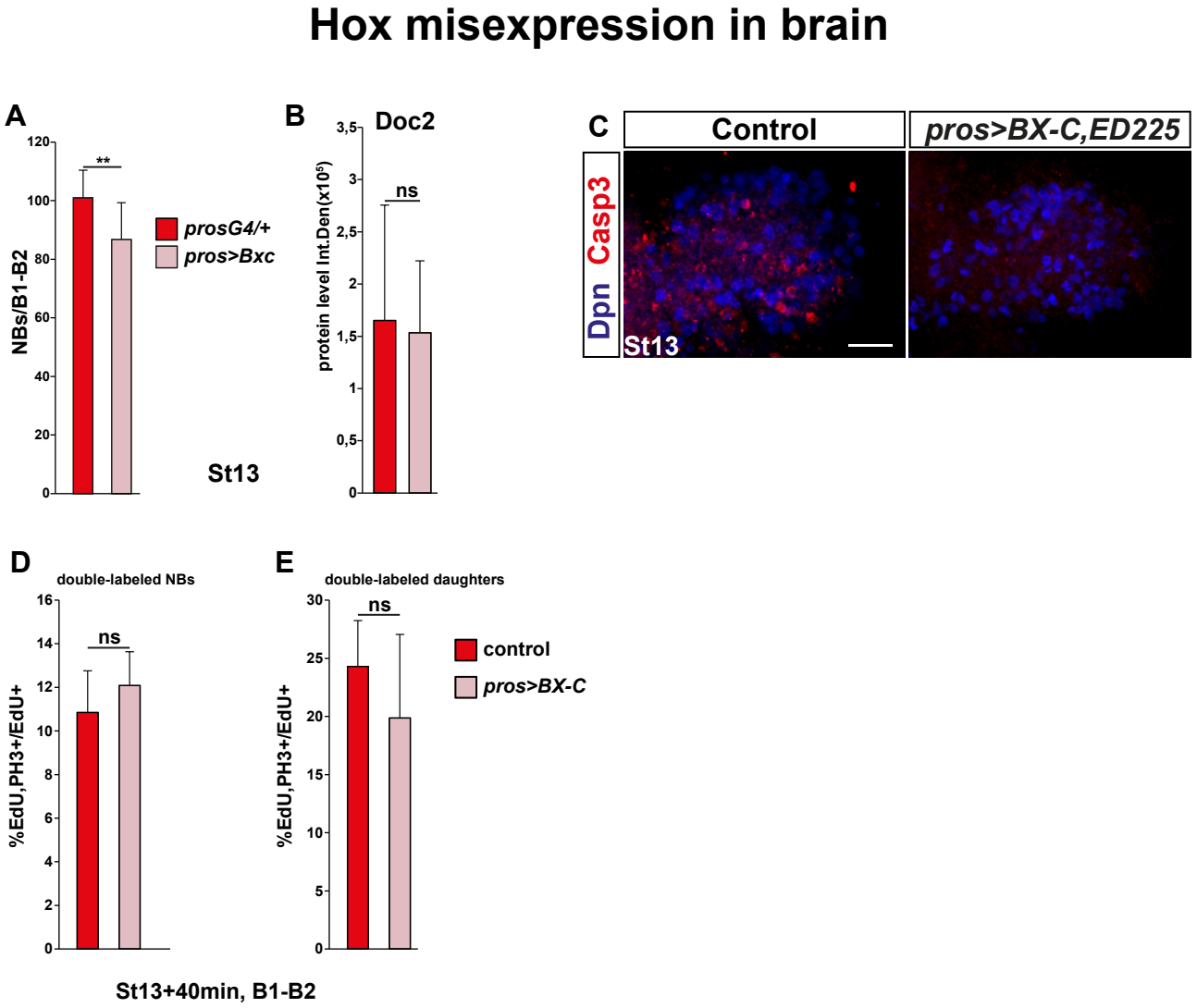

Figure S2.

Misexpression of *BX-C* reduces proliferation in brain daughters and NBs.
(A) Quantification of total NB numbers in B1-B2 in *prosG4/+* and *pros>BX-C*, at St13 (Student's t test; SD; n≥10 embryos per genotype). (B) Quantification of expression levels of Doc2 in B1-B2 NBs, at St13 in *prosG4/+* and *pros>BX-C* embryos (Integrated Density = area x mean gray value; Mann-Whitney U test; SD; n≥3 embryos, n≥248 NBs per genotype). (C) z-Projection images showing expression of the cell death marker, cleaved-Caspase3, in St13 brain lobes of control and *pros>BX-C,ED225* (scale bar; 20µm). (D-E) Ratios of double-labeled (EdU+, PH3+) to only EdU+, NBs and daughters in B1-B2, at St13 after a 40-min EdU pulse in control and *pros>BX-C* embryos (Student's t test; SD; n≥10 embryos per genotype).

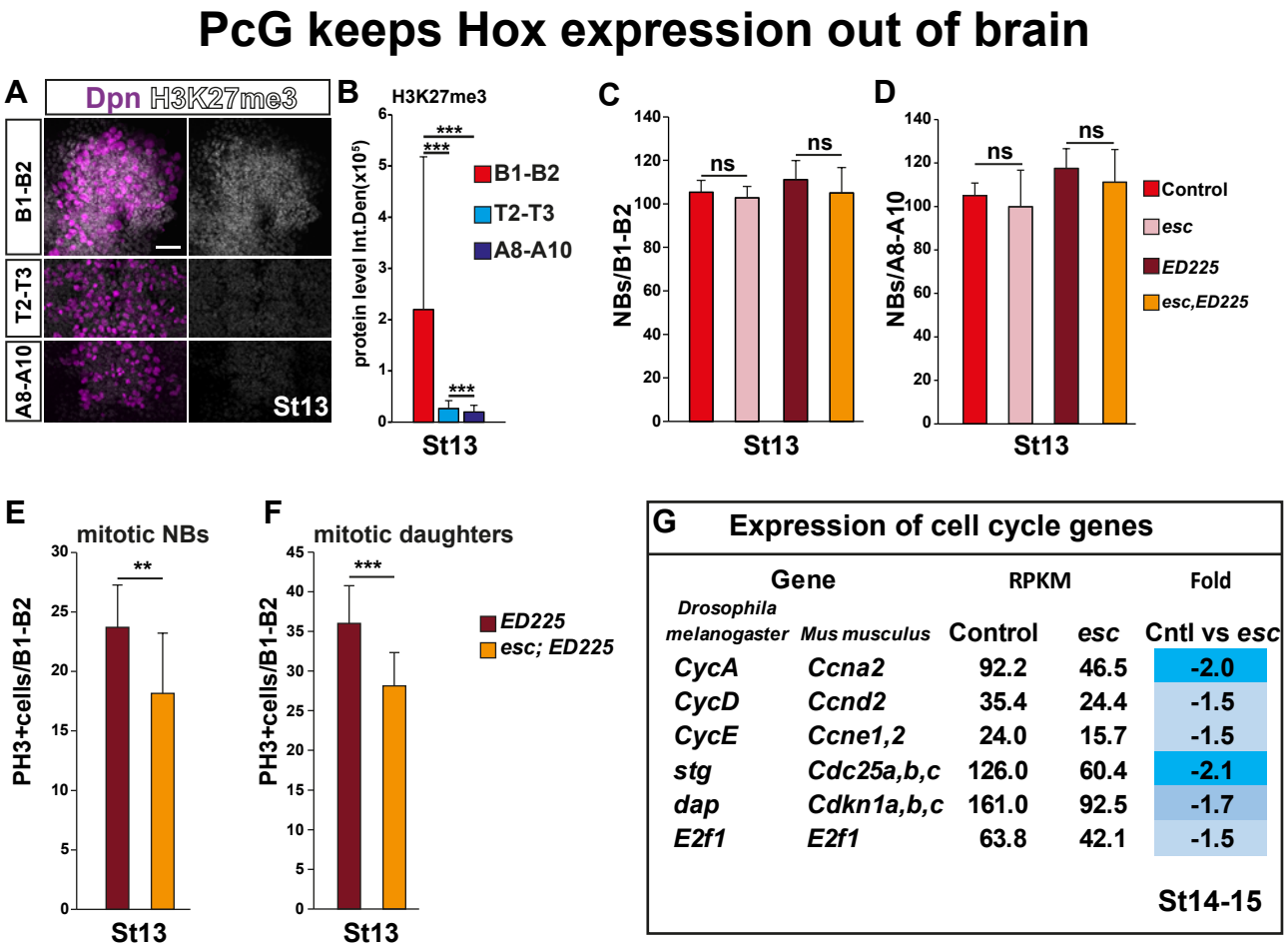

Figure S3.

Elevated H3K27me3 in brain, but no effect on NB numbers in *esc* mutants.

(A) z-Projections of H3K27me3 expression in B1-B2, T2-T3 and A8-A10, in St13 control embryos (scale bar; 20µm). (B) Quantification of H3K27me3 expression in NBs of St13 control embryos in B1-B2, T2-T3 and A8-A10 (Integrated Density = area x mean gray value; independent samples Kruskal-Wallis test, Mann-Whitney U test; SD; n≥3 embryos, n≥148 NBs per region). (C-D) Quantification of total NB numbers in B1-B2 and A8-A10, in control, *esc*, *ED225* and *esc;ED225* embryos, at St13 (Student's t test; SD; n≥6 embryos per genotype and region). (E-F) Quantification of mitotic NBs and daughters in B1-B2 in *ED225* and *esc;ED225* St13 embryos (Student's t test; SD; n≥8 embryos per genotype). (G) Whole embryo RNA-seq analysis of candidate cell-cycle genes in control and *esc* mutants. Columns from left to right; homologous genes in *Drosophila* and mouse, RPKM values in control and *esc* mutants, comparative *esc* to control fold changes (n=2 embryos per genotype, n=4 technical replicates per genotype, RPKM; reads per kilobases per million, FC; fold of change; FC>2;red, FC=1;white, FC<2;blue).

More dividing daughters in Telencephalon

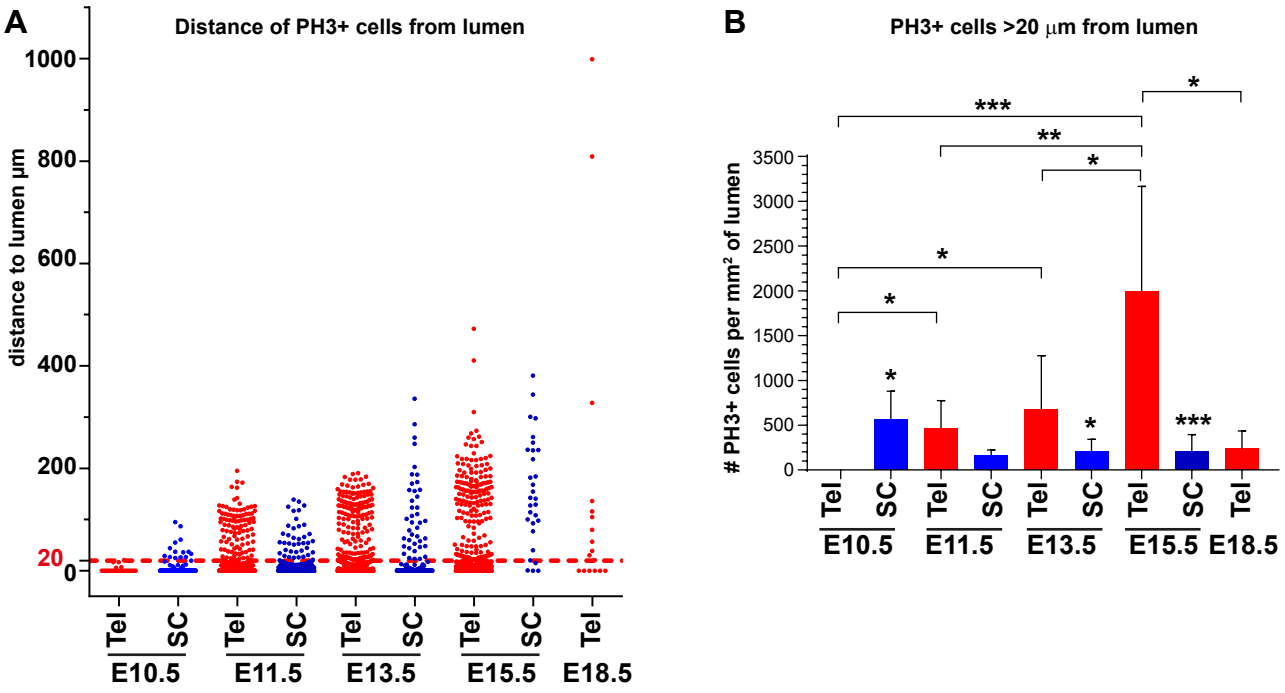

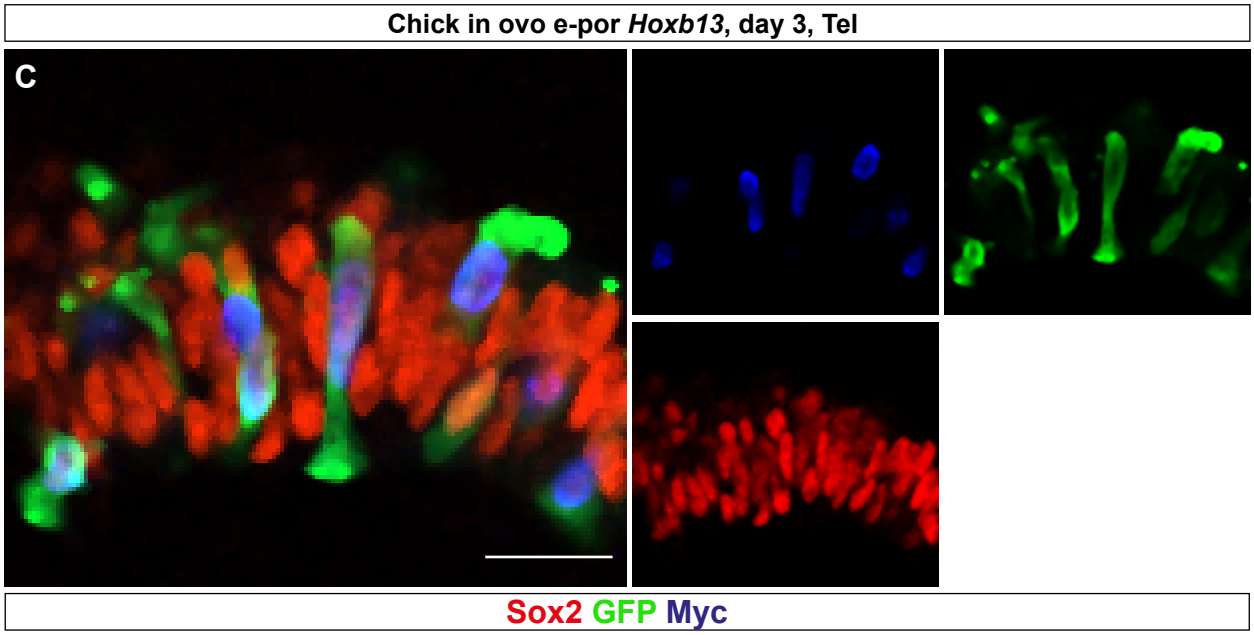

Figure S4.

Elevated daughter proliferation in telencephalon, and Hoxb13 misexpression.

(A) Position of mitotic cells in relation to the lumen, of Tel and SC tissues in control, at E11.5, E13.5 and E15.5 (red dashed line denotes 20 μm). (B) Number of mitotic cells in Tel and SC more than 20 μm distant from the lumen, normalized for luminal area (comparison at each stage using Mann-Whitney U-test; comparison between stages using Kruskal-Wallis with Bonferroni correction: SD; n≥3 embryos and 6-9 sections, 20-40 μm, per genotype and region). (C) Sox2, GFP and Myc staining of telencephalon to show co-electroporation of GFP and Hoxb13-myc plasmids in the chick embryo (scale bar = 20 μm).

Loss of H3K27me3 in *Eed-cKO* CNS

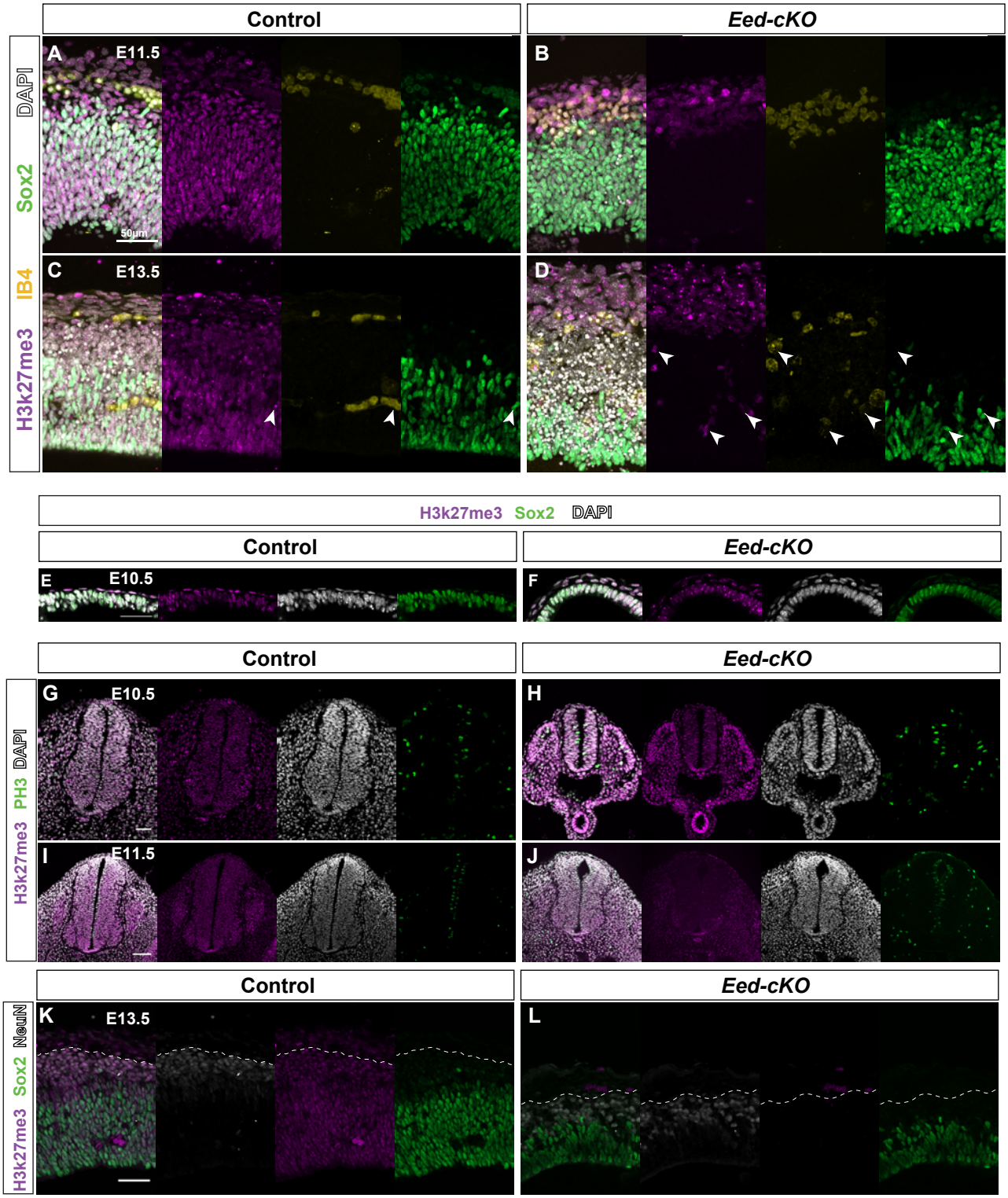

Figure S5.

H3K27me3 is lost in the CNS of *Eed-cKO* embryos, but still present in vascular tissue. (A-D) 12 to 18 µm confocal image projections of horizontal sections of Tel of control and *Eed-cKO* embryos stained for H3K27me3 and the vasculature marker IB4, at E11.5 (A-B) and E13.5 (C-D). *Eed-cKO* shows loss of H3K27me3 in the CNS proper, but staining is evident in vasculature (white arrows; scale bar = 50µm). (E-F) Staining for H3K27me3 in horizontal sections of Tel, of control and *Eed-cKO* embryos, at E10.5. *Eed-cKO* shows staining for H3K27me3 in the CNS proper (Sox2 cells; scale bar = 50µm). (G-J) Staining for H3K27me3 in horizontal sections of SC, of control and *Eed-cKO* embryos, at E10.5 (top) and E11.5 (bottom). The SC of *Eed-cKO* embryos shows reduced expression of H3K27me3 at E10.5 (H) and the expression is lost at E11.5 (J) when compared to control at the respective age (G, I) (scale bar = 50µm E-F, 100µm G-H). (K-L) Staining for the neuron-specific nuclear marker NeuN, which marks the outer-most layer of the CNS-proper/differentiated cells of CNS and H3K27me3 in horizontal sections of Tel, of control and *Eed-cKO* embryos, at E13.5. *Eed-cKO* shows no H3K27me3 in the CNS-proper when compared to control, but staining is evident outside the NeuN marker limit (15 µm projection confocal images, white dashed line; scale bar = 50µm).

Proliferation reduction in *Eed-cKO* CNS

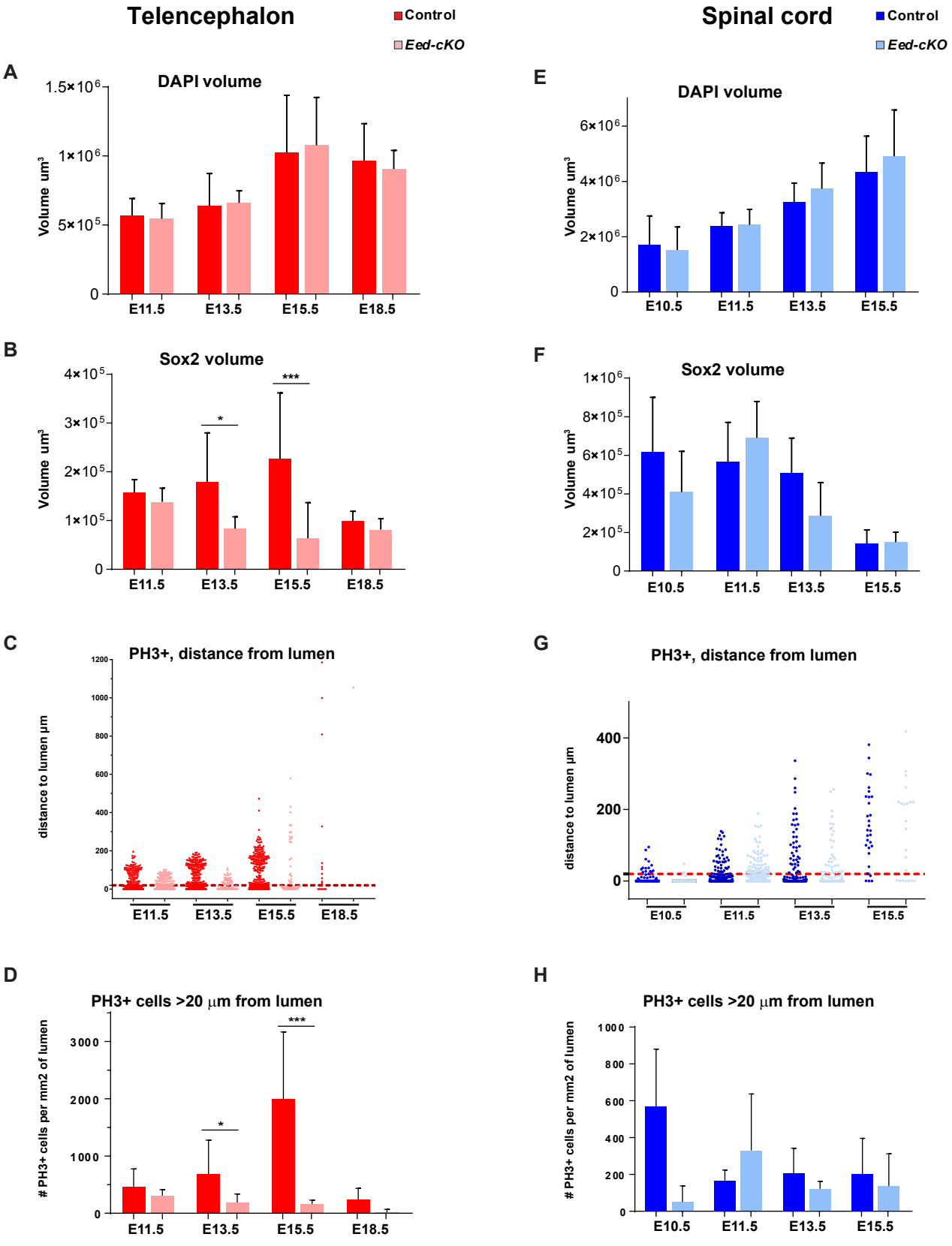

Figure S6.

Proliferation reduction in *Eed-cKO* embryos.

(A-B, E-F) Quantification of volume of DAPI and Sox2 signal in 200 µm bins along the lateral ventricles of horizontal sections, of Tel (A-B) and SC (E-F) tissues in control and *Eed-cKO* embryos at E10.5 (only SC), E11.5, 13.5, 15.5 and E18.5 (only Tel). (C, G) Position of mitotic cells in relation to the lumen, of Tel and SC tissues in control and *Eed-cKO* embryos, at E10.5 (only SC), E11.5, 13.5, 15.5 and E18.5 (only Tel; red dashed line denotes 20 µm). (D, H) Number of mitotic cells in Tel and SC more than 20 µm distant from the lumen, normalized for luminal area (comparison at each stage using Mann-Whitney U-test; SD; n≥3 embryos and 6-9 sections, 20-40 µm, per genotype and region).

p27 and PCD in telencephalon

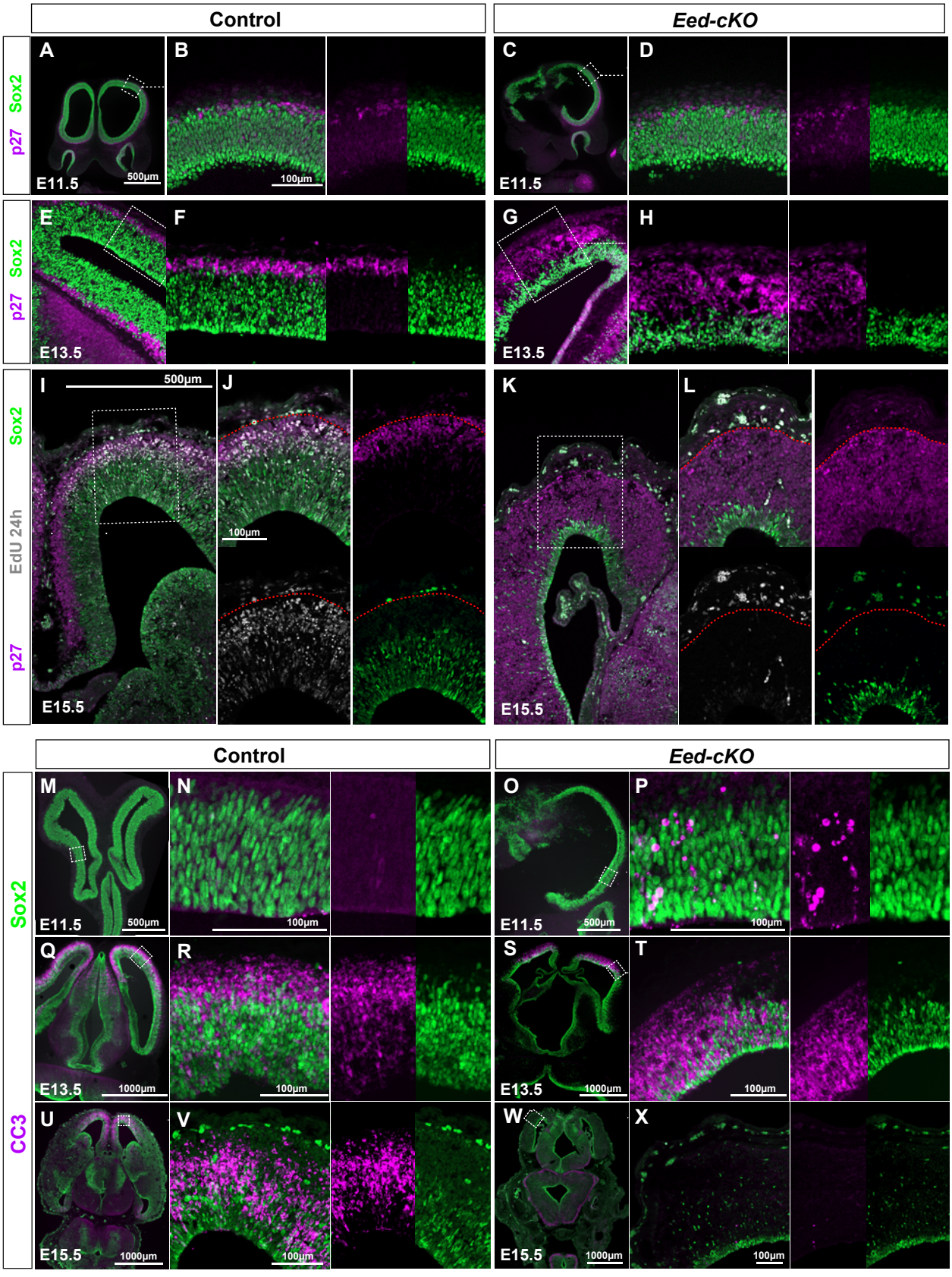

Figure S7.

Cleaved-Caspase3 and p27 expression in telencephalon.

(A-L) Staining for p27 and Sox2 in horizontal sections of Tel of control and *Eed-cKO* embryos at E11.5 (A-D), E13.5 (E-H) and E15.5 (I-L). Cell cycle progression is shown in white by EdU detection (24 hours pulse) at E15.5 (I-L). Red dashed lines indicate proper CNS/Tel tissue. Marked dashed square in A, C, E, G, I, K, indicate magnification area in B, D, F, H, J, L, respectively. (M-X), Staining for CC3 and Sox2 in horizontal sections of Tel of control and *Eed-KO* embryos at E11.5 (M-P), E13.5 (Q-T) and E15.5 (U-X). Marked dashed square in M, O, Q, S, U, W, indicate magnification area in N, P, R, T, V, X, respectively (overview panel scale bar; 500µm, insert panel scale bar; 100µm).

Expression of Cdc25C and E2F3 in Telencephalon

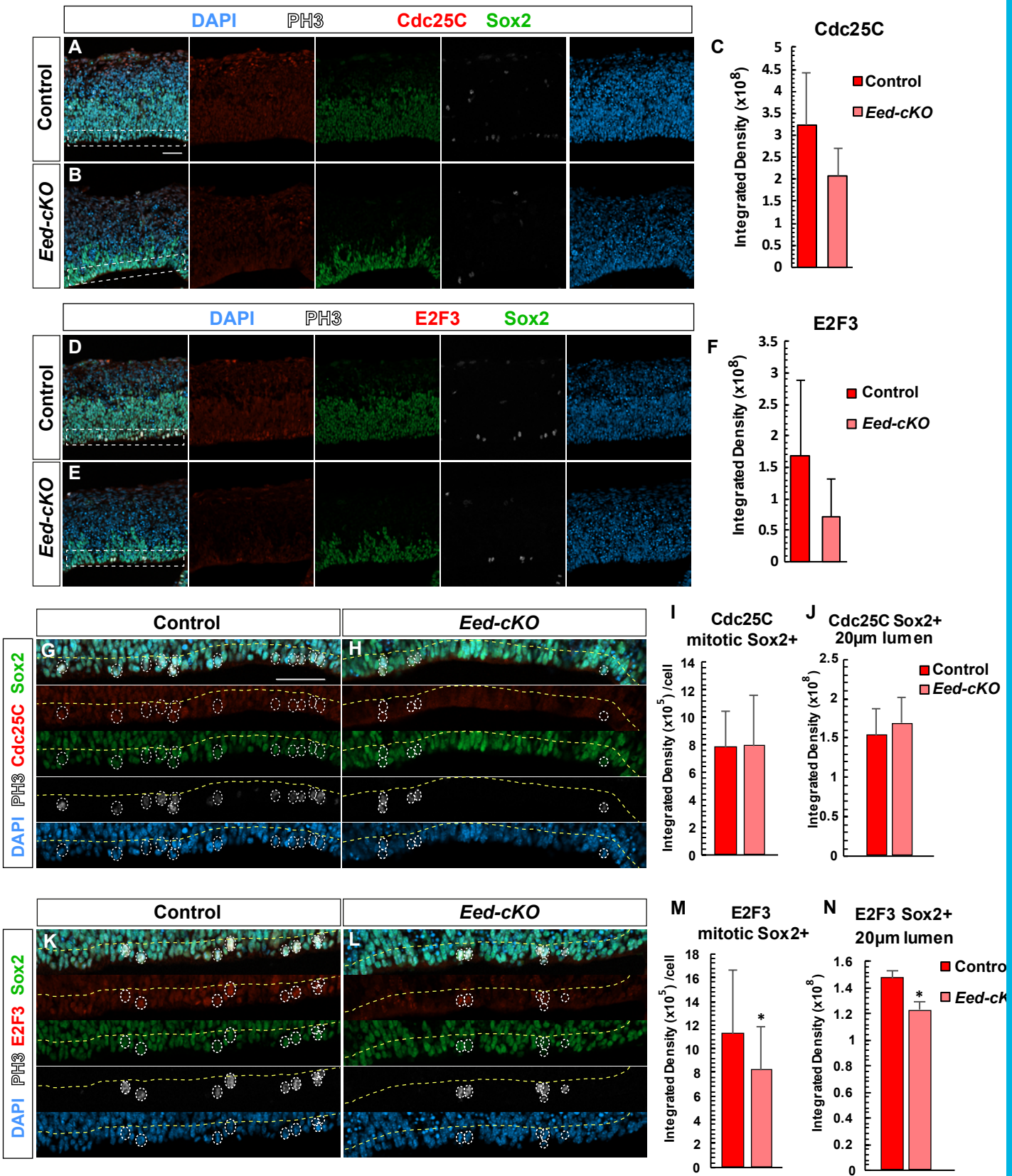

Figure S8.

Expression of cell cycle factors Cdc25C and E2F3 in telencephalon and spinal cord in *Eed-cKO*.

(A-B, D-E, G-H, K-L) Staining for Cdc25C and E2F3 in horizontal sections of Tel of control and *Eed-cKO* embryos, at E13.5, on the same slide for comparison. (C, F) Quantification of the Integrated density of Cdc25C (C) and E2F3 (F), showed reduced staining level, albeit not significant, in *Eed-cKO* embryos when compared to control. Square dashed lines indicate magnification areas showed in G-L respectively (scale bar; 50µm). (G-H, K-L) Magnification of the lumen area showed in (A-B, D-E) horizontal sections of Tel stained for Cdc25C and E2F3 in control and *Eed-cKO* embryos, at E13.5, on the same slide for comparison. Yellow dashed line show 20 µm from the lumen border area, white dashed line highlight mitotic progenitors. (I-J, M-N) Quantification of integrated intensity of Cdc25C and E2F3 was performed in progenitors (Sox2 positive) within 20 µm from the lumen border and in mitotic progenitors (Sox2 and PH3 positive) in control and *Eed-cKO* embryos. Significant reduction of E2F3 levels were revealed both for progenitors close to the lumen area (M) and for mitotic progenitors (N) in *Eed-cKO*, when compared to control.

p27 and CC3 expression in the Spinal Cord

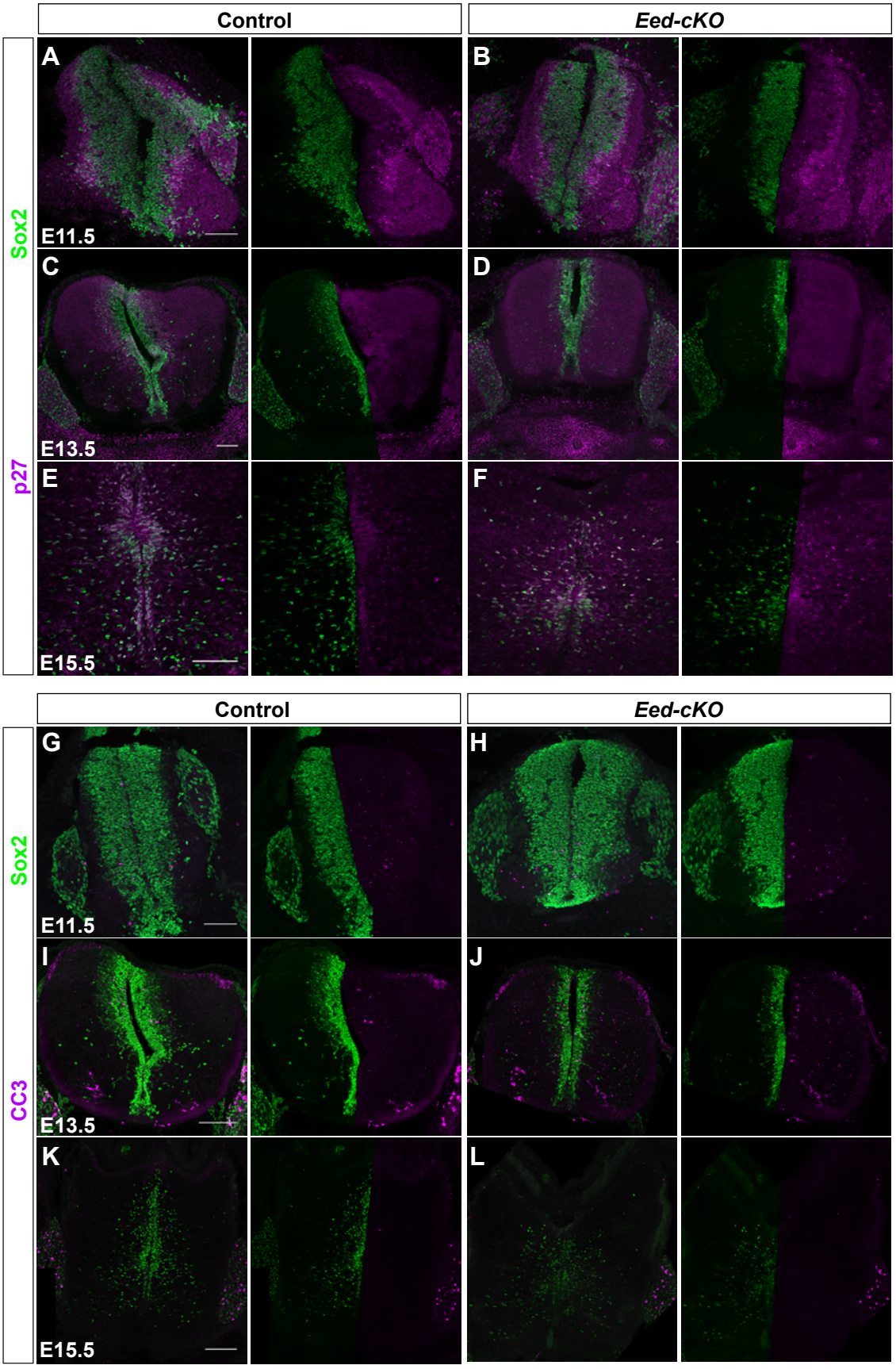

Figure S9.

Cleaved-Caspase3 and p27 expression in mouse spinal cord.

(A-F) Staining for p27 and Sox2 in horizontal sections of spinal cord of control and *Eed-cKO* embryos at E11.5 (A-B), E13.5 (C-D) and E15.5 (E-F) (scale bar; 100µm). (G-L) Staining for CC3 and Sox2 in horizontal sections of spinal cord of control and *Eed-cKO* embryos at E11.5 (G-H), E13.5 (I-J) and E15.5 (K-L) (scale bar; 100 µm G-H, 500 µm I-L).

Tbr2/Eomes and Tbr1 expression in Telencephalon

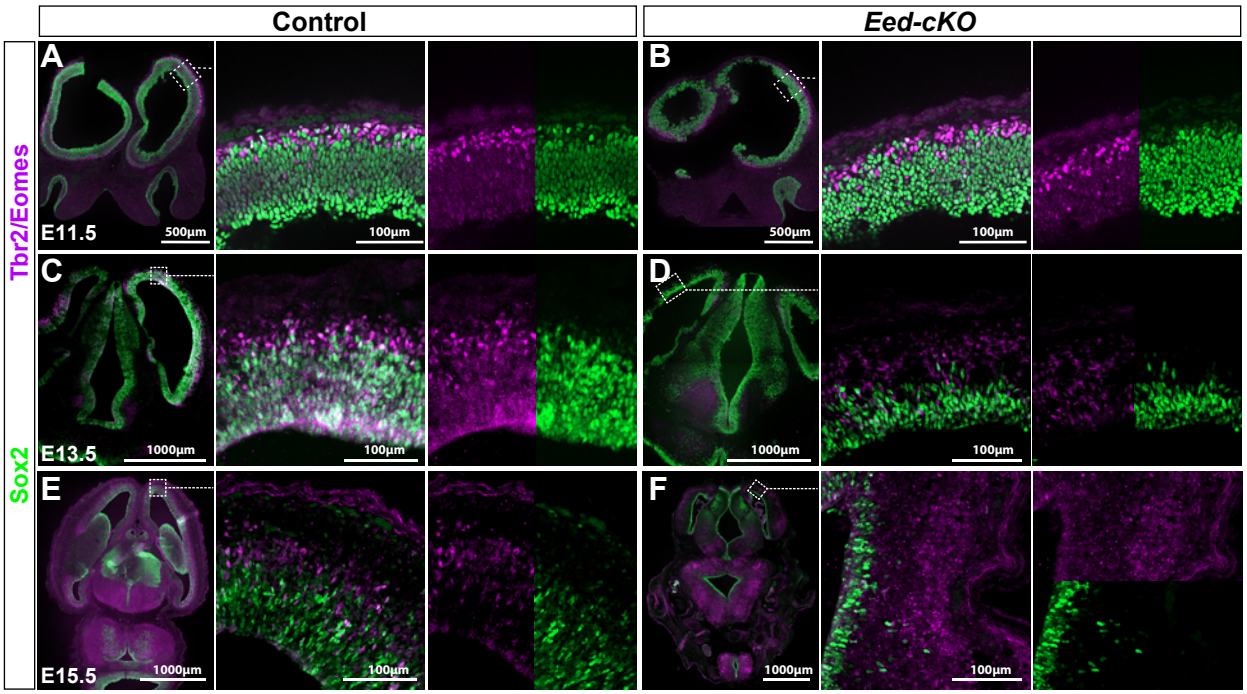

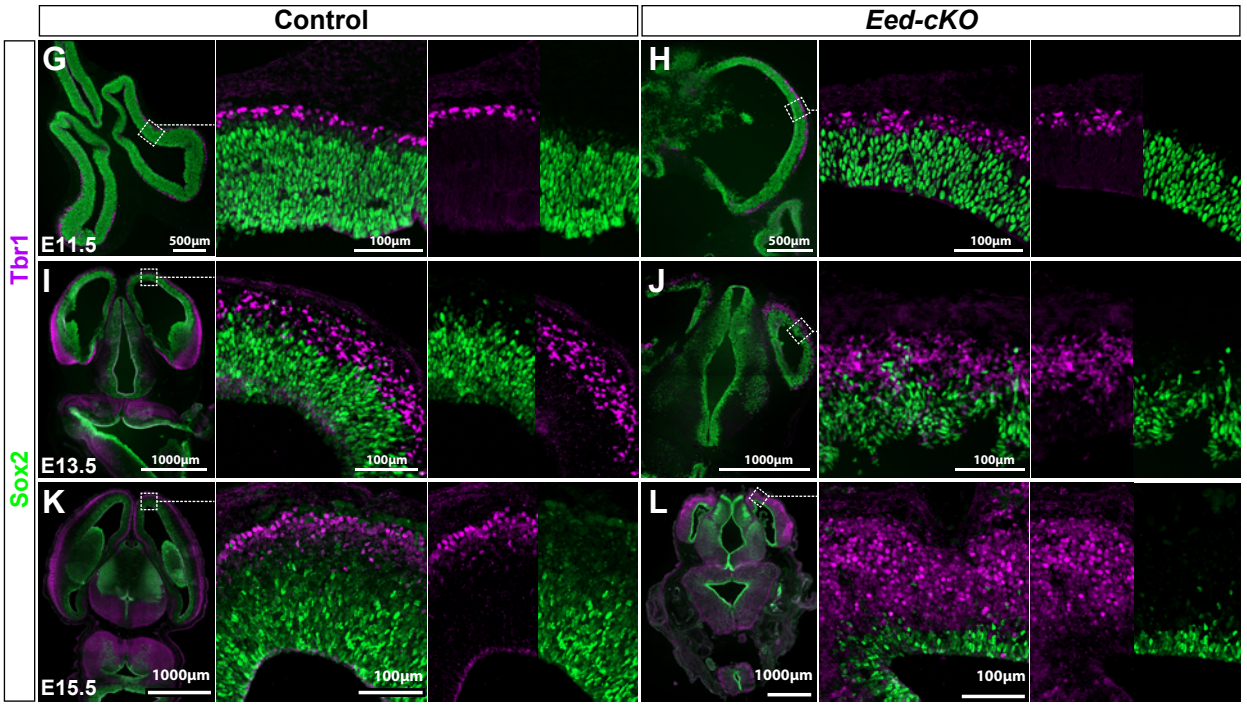

Figure S10.

Expression of Tbr1 and Tbr2 (Eomes) in the mouse telecenphalon.

(A-F) Staining for Sox2 and Tbr2/Eomes in the developing telencephalon, at E11.5, E13.5 and E15.5, in control and *Eed-cKO*. At E11.5, Tbr2/Eomes expression is not strikingly different, while at E13.5 and E15.5 there is a marked decrease in strongly expressing cells in *Eed-cKO*. (G-L) Staining for Sox2 and Tbr1 in the developing telencephalon, at E11.5, E13.5 and E15.5, in control and *Eed-cKO*. At E11.5, Tbr1 expression is not strikingly different, while at E13.5 and E15.5 there is a marked increase in strongly expressing cells in *Eed-cKO*.

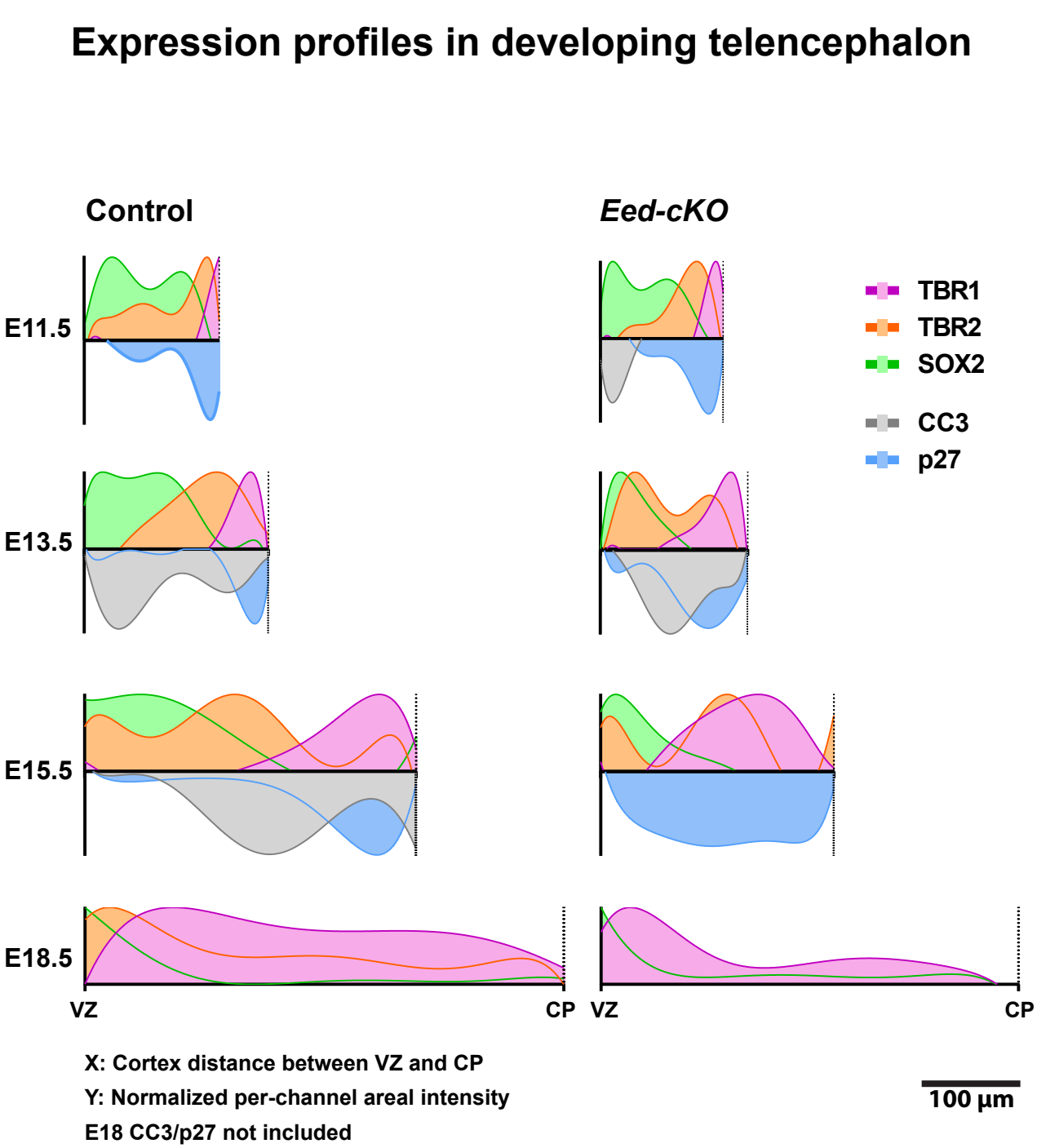

Figure S11.

Staining profiles of mouse telecenphalon.

Comparative telencephalon thickness during development, and zones of highest signal intensity of Sox2 (green), Tbr2/Eomes (orange), Tbr1 (lavender), Cleaved-caspase 3 (CC3; grey) and p27 (blue). Y-axes: intensity is per-channel ratio-normalized and range-normalized across all three channels, in arbitrary units (0 to 1, and inverted 0 to 1); X-axes: average tissue length between ventricular zone (VZ) and cortical plate (CP) of 7-26 measurements per age and genotype, to scale (µm).

Supplementary Materials and Methods

Supplemental DNA sequences

DNA sequences for optimized Hoxb9 and Hoxb13. Start ATGs underlined and bold.

Hoxb9:

gaattcgccgccacc**ATG**GCCGAGCAGAAGCTGATCAGCGAGGAGGACCTGGGACCACCTGGAATGTCCA
TCTCTGGCACCCTGAGCAGCTACTACGTGGACTCCATCATCTCTCACGAGAGCGAGGATGCCCCACCCGC
TAAGTTCCCTTCCGGACAGTACGCTAACCCAAGGCAGCCTGGACACGCTGAGCACCTGGATTTCCCAAGC
TGCTCCTTTCAGCCAAAGGCTCCCGTGTTTGGAGCTAGCTGGGCTCCTCTGTCCCCACACGCTTCTGGAA
GCCTGCCATCCGTGTACCACCCATACCTCCAGCCTCAGGGCGCCCCAGCCGCTGAGAGCAGATACCTGAG
AACATGGCTGGAGCCTGCTCCAAGAGCTGAGGCTGCTCCAGGACAGGGACAGGCCGCTGTGAAGGCTGAG
CCACTGCTGGGCGCTCCTGGAGAGCTGCTGAAGCAGGGCACCCCTGAGTACTCCCTGGAGACATCTGCCG
GACGCGAGGCTGTGCTGTCTAACCAGAGGGCTGGCTACGGAGACAACAAGATTTGCGAGGGATCTGAGGA
CAAGGAGAGACCAGATCAGACCAACCCAAGCGCCAACTGGCTGCACGCTCGGTCTAGCCGCAAGAAGAGG
TGTCCCTACACCAAGTACCAGACACTGGAGCTGGAGAAGGAGTTCCTGTTTAACATGTACCTGACACGGG
ATAGGAGACACGAGGTGGCCAGACTGCTGAACCTGAGCGAGCGGCAGGTGAAGATTTGGTTCCAGAACCG
GCGCATGAAGATGAAGAAGATGAACAAGGAGCAGGGCAAGGAGtaatgatagtctagagaattc

Hoxb13:

gaattcgccgccacc**ATG**GCCGAGCAGAAGCTGATCTCCGAGGAGGACCTGGGACCACCTGGAATGGAGC
CAGGCAACTACGCTACCCTGGACGGAGCCAAGGATATCGAGGGACTGCTGGGAGCTGGAGGAGGCCGGAA
CCTGGTGAGCCACAGCTCCCCTCTGGCTTCCCACCCCGCCGCTCCTACCCTGATGCCAACAGTGAACTAC
GCTCCCCTGGATCTGCCTGGCTCCGCCGAGCCACCAAAGCAGTGCCACCCATGTCCTGGCGTGCCTCAGG
GAGCTTCTCCAGCTCCCGTGCCTTACGGATACTTCGGAGGCGGATACTACAGCTGCCGGGTGTCCCGCTC
TAGCCTGAAGCCATGTGCCCAGACCGCTACACTGGCCACCTACCCCTCTGAGACACCAGCTCCAGGAGAG
GAGTACCCAAGCAGGCCCACAGAGTTCGCCTTTTACCCTGGCTACCCTGGACCATACCAGCCAATGGCTT
CTTACCTGGACGTGAGCGTGGTGCAGACCCTGGGCGCCCCTGGAGAGCCAAGACACGACTCCCTGCTGCC
AGTGGATTCTTACCAGCCCTGGACACTGGCTGGCGGATGGAACTCTCAGATGTGCTGTCAGGGCGAGCAG
AACCCTCCAGGACCCTTCTGGAAGGCCGCTTTTGCTGAGCCTAGCGTGCAGCACCCACCTCCAGACGGAT
GCGCCTTTAGGAGAGGAAGGAAGAAGAGAATCCCCTACTCCAAGGGACAGCTGAGGGAGCTGGAGAGGGA
GTACGCCGCTAACAAGTTCATCACCAAGGATAAGAGGAGGAAGATCAGCGCCGCCACCAGCCTGTCTGAG
AGGCAGATCACAATCTGGTTTCAGAACAGGAGAGTGAAGGAGAAGAAGGTGCTGGCCAAGGTGAAGACAA
GCACCACACCTtaatgatagtctagagaattc